General Disclaimer

One or more of the Following Statements may affect this Document

- This document has been reproduced from the best copy furnished by the organizational source. It is being released in the interest of making available as much information as possible.

- This document may contain data, which exceeds the sheet parameters. It was furnished in this condition by the organizational source and is the best copy available.

- This document may contain tone-on-tone or color graphs, charts and/or pictures, which have been reproduced in black and white.

- This document is paginated as submitted by the original source.

- Portions of this document are not fully legible due to the historical nature of some of the material. However, it is the best reproduction available from the original submission.

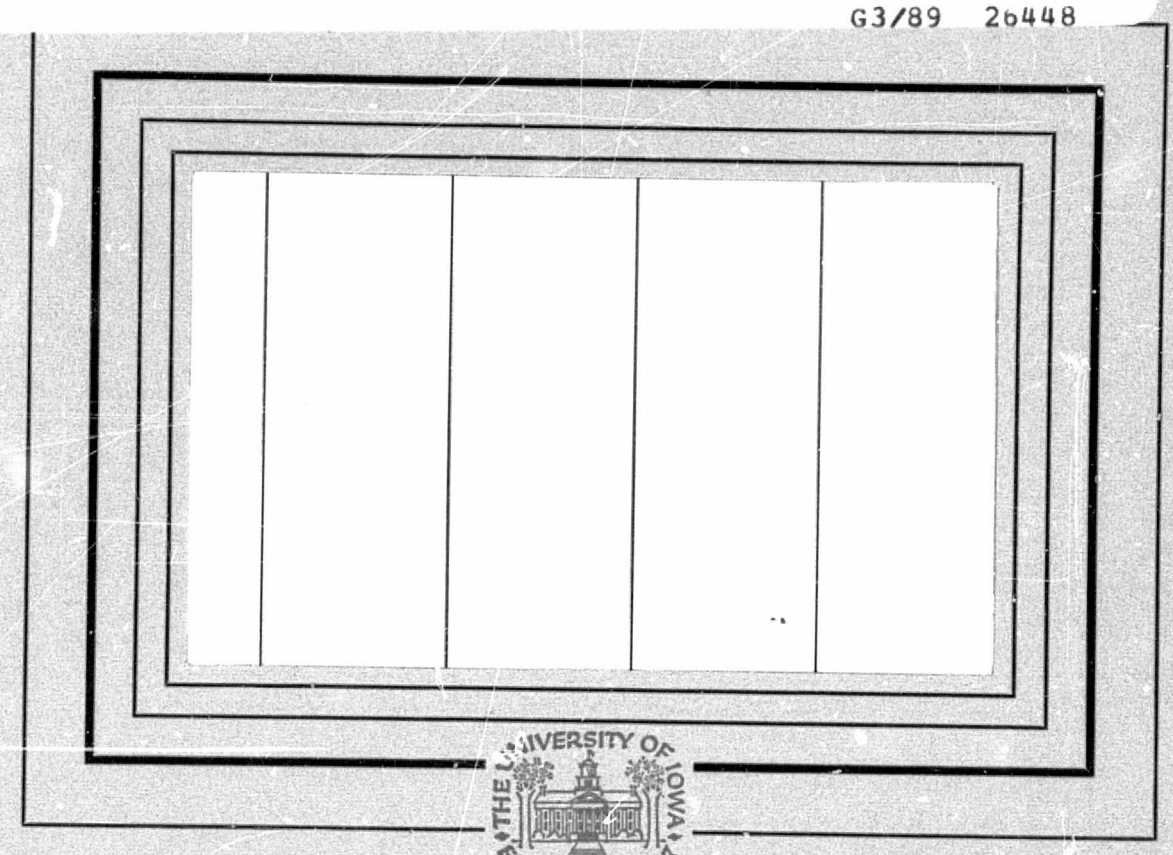

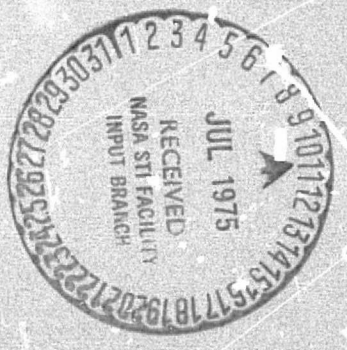

Department of Physics and Astronomy

THE UNIVERSITY OF IOWA

Iowa City, Iowa 52242

U. of Iowa 75-15

The 1973 Solar Occultation of The Crab Nebula Pulsar

by

Joel M. Weisberg

Department of Physics and Astronomy
The University of Iowa
Iowa City, Iowa 52242

May 1975

ABSTRACT

The mean electron density of the solar corona was determined by measuring the dispersion of radiofrequency pulses from pulsar NP 0532 during the June 1973 solar occultation. Observations were carried out at Arecibo Observatory. Trends continued which were noticed in 1971 as solar activity declined from its 1969 and 1970 levels: 17 $r_\odot$ east and west of the sun, 1971 path-integrated density was 50% greater; while 1973 density was approximately 80% greater than the corresponding 1969 and 1970 values; and yet 5 $r_\odot$ south of the sun, 1973 and 1971 integrated densities were only approximately one-half their 1969-70 values. A unique solution cannot be found by observing the occultation of a single object, but model fitting results suggest that the corona continued to become even more concentrated toward the equator in 1973 than in 1971. The equatorial number density of electrons at 10 $r_\odot$ was inferred to be approximately the same as in previous years (7500 cm^{-3}), while the number density of electrons in all other regions decreased. The decrease of density with radius also appeared still less steep in 1973 than in 1971, and markedly less than in 1969-70. The coronal multipath scattering delay, an index of coronal inhomogeneity, remained near its 1971 levels, less than one-tenth of its value in 1969-70.

The best model of the distribution of corona electrons is suggested to be one with zero density at the poles, which appears

consistent with the results of optical investigations during eclipses at a similar phase of the solar cycle. The best model is $\rho = 7500\ (r/10\ r_{\odot})^{-2.1} \cos^2\lambda\ cm^{-3}$, where λ is solar latitude. K-corona isophotes and contours of equal path-integrated density are presented for several models in order that other investigators may use their own criteria to judge which model is the most realistic. Extensive tables of electron density versus date and position in the corona are included for a variety of models.

A local enhancement of density and a local hole in the corona were observed in 1973. From an analysis of four occultations of NP 0532 it is seen that there is no simple relationship between the onset of major solar activity and density or scattering enhancements.

I. INTRODUCTION

In recent years the solar corona has been studied extensively by a variety of techniques. Each method has certain advantages and limitations. The purposes of this study are to refine the technique of determining the coronal electron density by observation of solar occultations of pulsars and to provide a means of calibration for other techniques.

A. The Techniques of Measuring Coronal Electron Density

Eclipse Photometry: During a solar eclipse the corona can be photographed out to a radial distance of at least 13 solar radii [Cox and Liebenberg, 1973]. The coronal light consists of two components: the K-corona which results from Thomson scattering of the sun's light by free coronal electrons; and the F-corona which is caused by the scattering of sunlight by dust in the ecliptic plane. In practice, the two components are separated by assuming that the emission from the K-corona is polarized, while the F-corona's light is assumed to be completely unpolarized.

However, recent calculations show that the F-corona may be slightly polarized [Newkirk, 1967]. Beyond 10 solar radii the radiance of the K-corona is so small that the inferred electron density would be altered drastically if even a minute portion of the F-corna's light

is indeed polarized. Thus the application of this technique is presently limited to radial distances less than 10 solar radii. Also, even in that region, it is difficult to distinguish coronal light from the sky background.

Radio Source Occultations: The scintillations of continuous radio sources as they are occulted by the corona can be used to measure the density fluctuations of the corona out to 80 solar radii. However, the interpretation of these fluctuations in terms of actual coronal density depends upon several uncertain assumptions regarding small scale scattering properties of the corona [Newkirk, 1967], such as alignment, scale size, and space-filling factor of the density fluctuations.

Direct Measurements: Spacecraft in heliocentric orbits have also carried instruments to directly probe the interplanetary medium [Hundhausen, 1972a]. Presently no in situ measurements have been made closer to the sun than Mariner 10's 0.4 a.u., although the Helios spacecraft will also directly measure the medium to within 0.3 a.u.

Radio Pulse Dispersion: An electromagnetic wave traveling through an ionized medium propagates with a group velocity that is a function of frequency and of the number density of free electrons. The difference in transit times at two frequencies is directly proportional to the electron number density integrated along the path. This technique has been used by spacecraft in heliocentric orbit

that receive pulses from the earth at two frequencies [Staff, Stanford Center for Radar Astronomy, 1966; Koehler, 1968]. Simultaneous radar observations of Venus at two frequencies have also been undertaken in order to measure the density of the intervening medium [Campbell and Muhleman, 1969]. Neither of these techniques has yielded information on the density of the medium closer than about 0.7 a.u. to the sun. Recently Mariner 10 data have presumably extended the range of dispersion measurements to within 0.4 a.u. Also the Helios spacecraft, launched in December 1974, will probe the medium as close as 0.3 a.u. from the sun with the dispersion technique.

Counselman and Shapiro [1968] suggested that the dispersion technique be used in conjunction with pulsars. It is this method that is used in the present work. Pulses from a pulsar are monitored as it is occulted by the corona. The relative delays of the received pulses at various frequencies can be used to determine the path-integrated electron density between the earth and the pulsar. The observed electron density is the sum of two components, one attributable to the corona and the other, to the interstellar medium between the observer and the pulsar.[1] The pulsar must be monitored at a wide range of solar elongations in order to separate the two components.

With the exception of the *in situ* measurements by spacecraft, each of the techniques yields only a line-of-sight integral of

---

[1] The contribution of the earth's ionosphere to the total observed electron density is approximately 10^{14} e^- cm^{-2} [Garriott *et al.*, 1965], which is entirely negligible.

electron density. Some assumptions about the geometry of the corona are necessary in order to determine the number density at a point in the corona.

B. Earlier Results from the Pulsar Dispersion Technique

The solar occultation of the Crab Nebula pulsar was observed from Arecibo in 1969, 1970, and 1971. The experiments yielded information on coronal densities in the region of 5-20 solar radii. The lower limit was fixed by the closest approach of NP 0532 to the sun. The upper limit was set by uncertainties in the (time-variable) interstellar electron content. The path integrated coronal electron density was 3.7×10^{16} e^- cm^{-2} at closest approach (5 $r_\odot$) of the earth-pulsar line to the sun in 1969 and 1970 [Counselman and Rankin, 1972]. For those years, when solar activity was at a peak, the corona was assumed to be spherically symmetric. Using such a model for the corona, the volume electron density was found to be:

$$\rho = 7000 \left(\frac{r}{10\ r_\odot} \right)^{-2.9} . \qquad (I.1)$$

In 1971 [Counselman and Rankin, 1973] the path integrated coronal electron density at 5 $r_\odot$ was only half of its 1969 and 1970 values. However, four days before and after the closest approach

of the pulsar-earth line to the sun, when the pulsar was 17 $r_\odot$ east and west of the sun, respectively, the 1971 integrated density was 50% greater than the corresponding values measured in 1969 and 1970. The 1971 model-fitting results yielded an equatorial density similar to 1969 and 1970 but indicated that the corona was highly concentrated toward the equator and that the logarithmic radial density gradient was less steep than in previous years. In 1971 the scattering due to coronal inhomogeneity also decreased markedly.

C. The 1973 Experiment

It was deemed useful to repeat the experiment in 1973 for several reasons. First, it is important to continue to monitor the changing nature of the corona through varying phases of the solar cycle. Second, substantial improvements in the experimental techniques had been made since 1971. A newly built digital pulsar anti-dispersing device [Boriakoff, 1973] had significantly increased the S/N available on the Crab Pulsar, and circularly polarized feeds had been mounted on the Arecibo radiotelescope in order to eliminate the possible timing errors due to the reception of a linearly polarized pulsar pulse by a linearly polarized antenna whose orientation changed through the observing period. Also, two pulsars were discovered which passed even closer to the sun than NP 0532 and within two weeks of the Crab occultation. Had we been able to observe them, the extra pulsars would have enabled us to refine greatly the shape

of the corona. Finally, R. M. MacQueen asked us to do the experiment to assist in interpretation of coronal observations of the Skylab mission. The orbiting laboratory carried a coronagraph which was designed to photograph the corona out to 6 solar radii. Because of the difficulties in interpretation of photographs of the corona mentioned above, it was hoped that our experiment could give a direct and unambiguous calibration of the line-of-sight coronal electron density recorded on their photographs.

II. EXPERIMENTAL DESIGN

A. Propagation of a Radio Wave in a Cold, Tenuous, Homogeneous Plasma

Let us first consider the properties of a pulse that is emitted simultaneously at two frequencies and which propagates through a cold, tenuous, homogeneous, and completely ionized medium. The quantities derived here form the theoretical framework for the experiment.

Rankin [1970] shows that the difference in arrival times at the two frequencies is:

$$t_1 - t_2 = \left(\frac{1}{\omega_1^2} - \frac{1}{\omega_2^2}\right) \frac{1}{2c} \int_{\text{path}} \pi^2 \, ds \qquad \text{(II.1)}$$

where ω_1 and ω_2 are the circular frequencies of the corresponding propagating waves and π is the electron plasma frequency in the medium. Rankin showed that terms of higher order which would normally appear in Eq. (II.1) may be neglected when observing NP 0532 in the frequency range of this experiment. Equation (II.1) may be rewritten:

$$t_1 - t_2 = D \left(\frac{1}{f_1^2} - \frac{1}{f_2^2}\right) \qquad \text{(II.2)}$$

where D is the dispersion constant, and f_1 and f_2 are the respective frequencies.

The dispersion contant is directly proportional to the path-integrated electron density, which is called the dispersior measure (DM).

$$DM = \int_{path} n_e(s)\, ds = \frac{8\pi^2 \epsilon_o mc}{e^2} D \quad . \tag{II.3}$$

Thus, in the case of a homogeneous medium, the path-integrated electron density can be determined by observation of the difference in arrival times of corresponding pulses at two different frequencies. However, small, irregular density fluctuations in the ionized medium between the pulsar and the earth complicate the situation. Their effects are discussed in the next section.

B. Refraction of the Wave Due to Density Irregularities

Radio scintillation measurements reveal the existence of small, irregular density fluctuations in the corona. The irregularities randomly scatter the radio waves from the pulsar. Erickson [1964] observed the apparent angular broadening of Taurus A as it was occulted by the corona and found the rms scattering angle in radians to be

$$\varphi_c = 1300\, f^{-2}\, R^{-2} \tag{II.4}$$

where R (in solar radii) is the solar impact parameter and f is the radio frequency in MHz. The effect of this random refraction is to further delay the peak of the pulsar because of the increased path length that must be traversed. The expected scattering delay, then, is

$$\langle \tau_S \rangle = \frac{a}{2c} (\varphi_o)^2 = 4.2 \times 10^{-8} \; f^{-4} \; R^{-4} \text{ sec MHz}^4 \; r_\odot^4 \qquad \text{(II.5)}$$

where a is the earth-sun distance.

Thus Eq. (II.2) is no longer strictly correct. The delay at each frequency is instead represented by a combination of dispersion and scattering effects:

$$\Delta t = Df^{-2} + Sf^{-4} \quad . \qquad \text{(II.6)}$$

Arrival-time measurements are required at a minimum of three frequencies in order to distinguish the dispersion and scattering delays. An expression of the form

$$t_{arr}(f) = t_o + Df^{-2} + Sf^{-4} \qquad \text{(II.6a)}$$

will be used to model the propagation delays. The observed arrival time at a given frequency is $t_{arr}(f)$. The three unknown parameters t_o, D, and S will be determined. The parameter t_o is the arrival

time of the pulse if the corona were not present. If the intrinsic timing of the pulsar is sufficiently stable, the predicted infinite-frequency (corona-free) arrival time may be included as an additional measurements.

C. Geometry of the Occultation

The path of the sun across the sky in the vicinity of the three pulsars is shown in Figure 1.

The pulsar dispersion method, like other line-of-sight techniques, yields the path-integrated electron density. In order to determine the electron density at a point, a model of the solar corona must be assumed. In 1969 and 1970 [Counselman and Rankin, 1972] a spherically symmetric model of the corona of the form

$$\rho = \rho_o \left(\frac{r}{r_o}\right)^{-\alpha} \tag{II.7}$$

was used. ρ_o and α were allowed to vary; r_o was fixed at 10 solar radii. This model must be modified at solar minimum when the corona is highly concentrated toward the equator [Newkirk, 1967]. The 1971 corona was modeled [Counselman and Rankin, 1973] with the addition of a term involving the solar latitude λ and a "flattening parameter", ϵ:

$$\rho = \rho_o \left(\frac{r}{r_o}\right) \left[1 - \epsilon\left(\frac{3}{2}\sin^2\lambda - \frac{1}{2}\right)\right] \quad . \tag{II.8}$$

This relation will be used for the 1973 corona. ρ_o, α, and ϵ are allowed to vary. However, as the inclination of the solar equator to the ecliptic is only 7°.25, it is impossible in practice to distinguish a latitude dependence of density (which would be reflected by the value of ϵ) from a radial distance dependence (which determines α) with a single occultation.[2] The discovery of pulsars JP 0540 and JP 0611 provided the hope of sampling the electron density along three distinct paths across the corona. Had such a possibility been realized, the true shape of the corona (and thus ϵ) could have been determined much less ambiguously.

---

[2] The passage of the pulsar south of the solar south pole occurs within a day of the closest approach of the pulsar to the sun. Thus variations in observed density during the occultation can be ascribed equally well to daily changes in the solar latitudes in which the (asymmetric) corona is sampled or to the different radial distances sampled each day.

III. EXPERIMENTAL EQUIPMENT AND TECHNIQUE

The experimental technique and equipment for the 1973 occultation were similar to those used in previous years. The important improvements are discussed extensively below, but only an outline of basic equipment and technique is given. For a detailed discussion of basic equipment and technique see Rankin [1970], Counselman and Rankin [1972], and Counselman and Rankin [1973].

A. The Telescope and Radiometers

The Arecibo radiotelescope is a 1000-foot diameter, fixed spherical reflector with traveling feeds. Any one of approximately ten different feed systems can be used by the experimenter. In order to differentiate scattering and dispersion this experiment requires observation of the pulsar simultaneously at three or more frequencies. A new circularly polarized feed system was constructed and tested for this experiment in the spring of 1973. This feed system replaced the linearly polarized array which had been used since the beginning of the Crab surveillance experiment in 1969. Thus any systematic errors due to reception of linearly polarized pulses by a linearly polarized feed whose orientation changes throughout the observations were reduced.

During the 1973 occultation experiment the surface of the Arecibo reflector was being replaced in order to upgrade its

capabilities. While the construction caused a significant increase in the power in the side lobes of the telescope as well as minor pointing errors, the experiment was not significantly degraded.

A block diagram of a typical radiometer is shown in Figure 2.

B. Special Requirements for Observing NP 0532

The sun passes 5 solar radii north of the Crab Nebula pulsar on June 14 or 15. Observations of NP 0532 are complicated by several factors. The pulsar is imbedded in the Crab Nebula, a noise source whose flux is two orders of magntidue greater than the pulsar's. Thus long integration times are required to detect NP 0532. In addition, NP 0532 has the shortest period (33 ms) of any pulsar. In order to achieve the time resolution required for this experiment, an extremely high data rate is required (120,000 samples/second). The problems were surmounted through the use of a synchronous sampling system. A Doppler-shifted ephemeris for the pulsar's period is used to determine a correct sampling rate which assures that consecutive pulses are added in phase by the on-line computer. Up to 32,000 consecutive pulses can be accumulated in this manner.

C. Interstellar Effects

The pulsar dispersion technique yields the electron density integrated along the path from the pulsar to the earth. It is necessary, then, to distinguish the interstellar contribution from that due to the corona. Unfortunately, the interstellar dispersion and scattering along the path to NP 0532 are time-variable

[Counselman and Rankin, 1971; Rankin and Counselman, 1973]. No other pulsar shows time variability of either scattering or dispersion.) Because of the magnitude and unpredictability of interstellar effects, no useful coronal information can be gained beyond approximately 20 solar radii, where the coronal dispersion and scattering are comparable to the uncertainties in the interstellar baseline.

In addition to delaying the pulse, the random refractions associated with interstellar scattering cause the pulse to become significantly broader at low frequencies. (See Figure 3.) Rankin and Counselman [1973] have studied this phenomenon extensively and find that the observed pulse broadening appears to occur in two different regions. It is postulated that one "screen" is the nebula itself, while the other consists of the interstellar medium between the solar system and the nebula.

D. Instrumental Effects

Rankin [1970] found that the pulses are also smeared by the receiver system itself. The three contributions are (a) the use of a finite bandwidth to observe a pulse sweeping in frequency, (b) the rise time of the filter used to limit the IF passband, and (c) the post-detection filter time constant. The effects can be minimized in order to achieve optimum time resolution but the resulting experimental configuration would require unacceptably long integration times for detection. Such considerations therefore have served only as a guide for the actual configuration which is listed in Table 1.

E. The Digital Antidispersing Device

In the spring of 1973 a digital antidisperser became available for pulsar observations at Arecibo Observatory [Boriakoff, 1973]. This device electronically adds the proper delays to each of 32 consecutive 20 kHz channels so as to remove dispersion across the passband. The result is a signal of 640 kHz bandwidth whose characteristic smearing is only that of a dispersed pulse sweeping through a 20 kHz filter. A significant increase in S/N results from use of a bandwidth much wider than would otherwise be possible.

F. Allocation of Frequencies

The antidisperser can be used at any frequency. Considerable effort was expended in finding the optimum one.

The computer can sample each of eight data channels every 64 μsec. There is considerable freedom in experimental design, with four observing frequencies, one antidisperser, and eight data channels sampled at 64 μsec intervals. The characteristics of a multitude of experimental configurations were examined.

There are several important criteria to be optimized. Certainly the most accurate value of the dispersion constant D is highly desirable. However, it is also important to minimize the correlation between the dispersion and scattering parameters D and S, as well as between the dispersion and the infinite-frequency baseline (t_o).

It is possible to simulate the various experimental configurations and determine the expected correlations and standard deviations

in D, S, and t_o without the use of actual data if the expected standard deviations of the data are known. Starting with the expected standard deviation in arrival times at each frequency, the normal equations can be inverted to yield the expected standard deviations in the parameters D, S, and C, as well as the correlations between them.

Typical standard deviations in arrival times for channels without the antidisperser were determined by analysis of NP 0532 arrival times at each frequency on several days in February 1973. The arrival times from 18-minute integrations were referred to a common epoch. The rms scatter in arrival times about the mean was calculated and called the expected standard deviation.

The expected improvement in the standard deviation in arrival times when the antidisperser is used at any frequency was determined through use of the Dicke equation (in which S/N is proportional to the square root of the bandwidth), and allowing for smearing in the individual 20 kHz channels.

Table 2 gives the expected standard deviation in arrival time for an 18-minute integration at each frequency, with and without the antidisperser. (The use of the antidisperser was not considered at 73.8 MHz because the 20 kHz filters in the antidisperser would individually smear the pulse too much.)

The expected standard deviations in Table 2 assume a 32 μsec sampling interval at 430 MHz; 64 μsec at all other frequencies. (A

smaller sampling interval is necessary at 430 MHz due to the intrinsically narrower pulse at that frequency.) Thus each 430 MHz radiometer actually requires two of the eight channels sampled by the computer at 64 μsec intervals.

The results of computer simulations based upon Table 2 indicate that the antidisperser is best employed at 196.5 MHz; with two regular channels each at 430.0 and 73.8 MHz, and one regular channel at 111.5 MHz.

IV. THE CORONAL OCCULTATION

A. The Pulsars

The two newly discovered pulsars were not detectable when they were occulted by the corona. Thus this experiment was limited to an occultation of the Crab Pulsar alone.

B. The Data

A typical day's data consists of from nine to twenty 18-minute integrations ("runs") at each frequency. The observing configuration suggested by the computer simulations was employed until June 13. At that time preliminary analysis indicated that little useful information was being recorded at 73.8 MHz. Therefore the second 73.8 MHz channel was replaced by a second 111.5 MHz channel. The typical configuration then consisted of two channels each near 430.0 and 111.5 MHz; one channel at 73.8 MHz; and the antidisperser at 196.5 MHz. A regular 196.5 MHz channel occasionally replaced the extra 111.5 MHz channel in order that the antidispersed 196.5 MHz data could be directly compared with regular 196.5 MHz data.

Figure 3 shows actual pulse shapes from 18-minute integrations on July 11 when the sun was remote from the pulsar; and June 15, near the time of closest approach of the two. The waveforms are significantly noisier on June 15. The dramatic improvement of the signal on the antidispersed channel (channel 3) over its conventional

196.5 MHz counterpart (channel 7) is obvious on both days. It can be seen that the antidisperser provides an extremely well-defined pulse shape whose phase is easy to measure.

C. The Preliminary Analysis

The first step in the analysis was to determine the arrival time of the pulsar's pulse for each 18-minute run. The experimental pulse was cross-correlated with a template pulse whose shape reflects both interstellar and instrumental smearing. The maximum of the cross correlation function defines the pulse phase and hence the pulse arrival time. In addition, the statistical properties of the cross correlation function can be used to estimate the probable error in arrival time at 430 MHz. (Experience has shown that there is no such relationship at the lower frequencies.)

Next, a best estimate of the arrival time for the whole day was calculated at each frequency in the following manner: The pulse arrival time for each run in a day at the given frequency was compared to the arrival time predicted by an ephemeris based on the pulsar's past performance. The daily mean of the residuals was then calculated. (At 430 MHz the mean was weighted according to the quality of the original arrival time estimations, while at the lower frequencies all runs were weighted equally.) The difference between the daily mean residual and the residual of the observation made closest to transit on that day was added to the measured arrival time of the transit run. This "phase average" of the daily pulse arrival time

at each frequency was then weighted according to the scatter of residuals within that day.

Individual runs whose arrival times differed by several standard deviations from the average were then carefully examined. Many could be reclaimed by re-examining their cross correlation with the template pulse and identifying and rejecting noise peaks. At this stage the phase of the 73.8 MHz arrivals on each day was found to be essentially random. No further analysis of 73.8 MHz observations was undertaken.

The daily phase-averaged arrival times at each frequency were next used to make an improved pulsar pulse arrival ephemeris. An improved set of daily phase-averaged arrival times was then obtained by again comparing each run in a day at a given frequency with the predictions of the improved ephemeris. This procedure was iterated several times until a highly consistent set of arrival times on each day was generated.

Figures 4, 5, and 6 show the residuals to a quartic fit in pulsar phase for 430, 196.5, and 111.5 MHz, respectively. Figure 7 displays the three curves, all plotted with the same scale. Data from June 8 through 21 were not weighted in the fit. The data points represent the "best" arrival time estimate; the error bars represent the rms scatter of a day's runs about the mean. The baseline of the quartic fit can be taken to represent both the smoothed intrinsic timing of the pulsar and timing variations that are caused by

changes in interstellar dispersion; any significant deviations from it are either due to timing irregularities in the pulsar or to the solar corona. (The characteristic time scale of interstellar dispersion changes is sufficiently long to enable a quartic fit to model them accurately.) It is uncertain whether the broad maximum in Figure 4 which lasts from May 26 to July 4 is the result of dispersion delay in the outer corona or of pulsar timing irregularities. Because the (corona-free) baseline in Figures 4 through 7 could not be established reliably, coronal dispersions could not be determined from delays relative to the baseline. Instead, timing differences between the various frequencies were used to determine the total (interstellar and coronal) dispersion; and the interstellar component was removed at a later stage of the analysis. (See below.)

Loss of the 73.8 MHz data tended to indicate an increase in the strength of the second interstellar scattering screen, which had long been quiescent [Rankin and Counselman, 1973]. The data at all frequencies were therefore cross correlated with templates which reflected smearing due to two interstellar screens instead of the one screen model which was used in the original analysis. However, when the arrival times determined from a double screen model of the interstellar medium were used to find daily phase-averaged arrival times, they were found to be less consistent than those based upon a single screen model. Thus the lack of precision in the 73.8 MHz measurements can not be explained in terms of increased interstellar

scattering. Analysis of recent measurements indicates that the flux of NP 0532 at low frequencies has decreased significantly within the last few years [Rankin, Payne, and Campbell, 1974]. This is a likely explanation of our difficulties at 73.8 MHz.

D. Path-Integrated Electron Density, and Scattering Delay

A linear weighted least squares fitting technique was used to fit the daily average arrival times at 430.0, 196.5, and 111.5 MHz to a model of the form of Eq. (II.6a). Table 3 and Figures 8 and 9 display the results. The total dispersion parameter, D, is plotted against time in Figure 8. (Recall that 1 sec MHz^2 corresponds to 0.743×10^{15} e^- cm^{-2}.) At this stage it is evident that it is difficult to separate the interstellar dispersion from the component of dispersion that is attributable to the corona. In Figure 9 the scattering parameter S is shown. The only significant scattering enhancements occur on June 12 and 14.

E. The Three-Dimensional Electron Density Distribution of the Corona

1. The Coronal Model

In the previous section the technique for determining the total path-integrated electron density (D) was described. The parameter D requires no assumptions about the distribution of the corona; in this sense it may be considered an observable quantity. In order to derive any information on the density at a point in the corona,

however, one requires some coronal model over which to deconvolve the path-integrated variables. The model used in this work, Eq. (II.8), includes a dependence upon solar latitude λ and flattening parameter ϵ. The exact form of the model's dependence upon these two parameters is rather arbitrary. The importance of Eq. (II.8) lies in the fact that ϵ and λ allow for any asymmetric density distribution as is expected near the time of solar cycle minimum. As Counselman and Rankin [1973] point out, such a model should not be taken too literally since it is the result of a set of observations based upon only a limited number of rays directed through the corona. While our model may not match the details of the actual coronal electron density distribution, we believe that its general form permits us to perform two important tasks:

(a) We can subtract the interstellar dispersion from our measuremens in a realistic manner [see (2) and (3) below]; and

(b) We can infer at least qualitatively the variation of electron density with solar latitude.

It should be noted that the model does not permit a variation of density with solar longitude, and thus implicitly represents an average over longitude.

2. The Interstellar Model

Equation (II.8) alone is not sufficient to model successfully the observed variation of path-integrated electron density (D) with time. The interstellar dispersion was also time-variable. Consequently the interstellar dispersion D_I was assumed to vary as

$$D_I = D_o + D_1(t - t_o) + \frac{1}{2} D_2(t - t_o)^2 \qquad \text{(IV.1)}$$

(t_o was June 15).

3. Results

Iterative weighted least squares were used to find simultaneously the three background parameters D_o, D_1, and D_2, as well as the coronal parameters ρ_o and α. All data points listed in Table 3 and shown in Figure 8 were weighted in the fit. Since our measurements could not separate α and ϵ, a series of solutions was calculated in which ϵ was fixed at various values from 0 (representing a spherically symmetric corona) to 1.4 (electron density set to zero for all solar latitudes greater than 64.°1 north and south). The results of the various fits are shown in Table 4. In all cases the value of the parameter χ^2 is considerably larger than that expected for statistically-independent observation errors. (In 1971 the value of χ^2 reflected only independent errors.)

For the 1973 models with ϵ ranging between 0 and 1.0, the larger value of χ^2 is ascribable to the significantly improved ($\sim 0.5x$) standard deviations in D which are the result of the use of the anti-disperser. Thus the 1973 residuals reflect an actual phenomenon whose variation is not being modeled. Nevertheless, no further parameters were added to the model. Figures 10 and 11 show the $\epsilon = 0.6$ and 1.0 models, respectively, as well as the experimental data. With the exception of two large transient variations, the experimental data

appear to follow the model adequately. It would be unrealistic to attempt to model local density variations in the corona on the basis of our line-of-sight measurements. Therefore the present form of the model is considered sufficient, and the poor fit is ascribed to (real) local density variations.

The value of χ^2 increases further for models with ϵ greater than 1.0. These highly flattened models have no electrons at all at polar latitudes. The poorer fit is ascribed to the fact that there is no evidence in the data for the dip in path-integrated electron density expected in the extremely flattened models near mid-occultation as the pulsar passed near the solar south pole. (See Figure 12, which shows the $\epsilon = 1.4$ model as well as the experimental data.)

An independent means of determining the value of ϵ is obviously very important. Unfortunately instrumental difficulties have delayed the reduction of Skylab coronagraph observations. C. F. Keller of Los Alamos Scientific Laboratory is also in the process of determining K-corona isophotes from photographs taken from an NC-135 aircraft during the June 30 eclipse. When these data become available it is expected that the value of ϵ can be determined unambiguously. At that time the ambiguous results of Table 4 can be replaced by a best coronal model. Until then it is necessary to use less direct arguments to determine the value of ϵ.

First, it is known that the corona becomes highly concentrated toward the equator during solar cycle minimum. Photographs from the June 30 eclipse as well as Skylab coronagraph observations indeed depict a highly flattened corona.

Second, present models of the corona predict that the solar wind velocity is increasing in the region from 5-20 $r_\odot$ [Hundhausen, 1972b]. Therefore, as a result of the requirement of conservation of mass, values of α less than 2.0 are excluded. This stringent criterion rules out models with ϵ less than 0.6, even if a one standard deviation error in the value of α is permitted.

Third, when extrapolated to 1 a.u., all but the more flattened models predict an unrealistically high value for the electron density. This criterion must be qualified by noting that our measurements were carried out in a regime somewhat different than the interplanetary medium in the vicinity of the earth.

Fourth, as discussed previously, model fitting results suggest that it is unlikely that ϵ is greater than 1.0, although a local density enhancement on June 14 could have masked the decrease in polar path-integrated density which is predicted by the extremely flattened models but which was not observed.

Taken together, the evidence indicates that the corona was considerably flattened in June 1973, with $\epsilon \approx 1.0$. However, more flattened models can not be ruled out.

Table 5 lists the calculated total dispersion and interstellar baseline for ϵ = 0.4, 0.6, 0.8, 1.0, 1.2, and 1.4. The values in Table 5 are based upon the fits listed in Table 4. The observed coronal electron column densities for a given value of ϵ correspond to the difference between the interstellar background on any date and the observed total dispersion. Likewise, for a given value of ϵ,

the difference between the interstellar background on any date and the calculated total dispersion yields a "smoothed" value of coronal electron column densities. (The variation of the values of the interstellar parameters D_o, D_1, and D_2 with ϵ in Table 4 makes it clear that even coronal column densities require a knowledge of ϵ in order to subtract the correct interstellar contribution. Figures 13-18, which are discussed extensively in the next paragraphs, are included specifically in order that other investigators can choose a best value of ϵ based upon their own criteria.)

Figures 10-18 portray the best fitting coronal models for ϵ = 0.6, 1.0, and 1.4, based upon Table 4. Figures 10-12 show the measured coronal dispersion and the best fitting models of dispersion versus time for the three values of ϵ. In Figures 13-15 contours of equal path-integrated coronal electron density are plotted on the basis of the best fitting models for the selected values of ϵ. And K-coronal isophotes of the best fitting models for the three values of ϵ are shown in Figures 16-18. The isophotes were calculated on the assumption that the K-corona results from the Thomson scattering of sunlight by electrons distributed according to our coronal models. The inverse-square dependence of the flux of sunlight and an anisotropic Thomson scattering law were included in the calculations. (Van de Hulst [1950] showed that solar limb darkening can be ignored safely in the region of interest.)

The position of the pulsar at Arecibo transit on each day in mid-June is also shown in Figures 13-18. It is clear that only a

small range of solar impact parameters and position angles has been sampled in this experiment. Thus our models are not definitive or accurate representations of the entire corona. The detailed contours shown for the entire corona in Figures 13-18 are included solely in order that other workers may use their own criteria to judge which of our models is the most realistic.

4. A Comparison With Earlier Investigations

Many groups have done optical studies of the corona during solar eclipse. Von Klüber [1958], Ney et al. [1961], and Gillett et al. [1964] carried out very careful experiments which should be compared with our results, despite the fact that their investigations of the K-corona did not extend out as far as 5 $r_\odot$, the minimum solar impact parameter probed in the present work.

Von Klüber observed the eclipse of 25 February 1952 from Khartoum, when the phase of the solar cycle was similar to its value during the present experiment. On the basis of his intensity and polarization measurements, and assuming a spherically symmetric corona in his calculations (but not in his results), he presented contours of equal electron density out to 3.5 $r_\odot$. The contours reveal a very low electron density at the poles, corresponding approximately to our $\epsilon = 0.9$ model.

Ney et al. observed the eclipse of 2 October 1959 from two stations in French West Africa, when solar activity was near maximum. They found that the K-corona appeared slightly concentrated toward

the equator even at solar maximum. A model of electron density was constructed to fit the observed K-corona in which the density was equal to its equatorial value at all latitudes up to some cutoff latitude, beyond which the electron density was zero. It was found that they could then fit their observations to a corona completely free of electrons beyond latitudes of 70°. By applying their model to von Klüber's 1952 eclipse data, Ney et al. found that no electrons were necessary within 25° of the poles (i.e., beyond 65° latitude).

Gillett et al., upon observing the eclipse of 20 July 1963 (also at a solar cycle phase similar to that of the present work), also found that a model of electron density with a density cutoff near the poles could fit their observed K-corona.

On the basis of the work of Ney et al. and Gillett et al. it is tempting to select our $\epsilon = 1.4$ model (in which electron density is zero beyond 64.1 latitude) as the best coronal model. However our models, in which the electron density is a smoothly-varying function of solar latitude, are a compromise between von Klüber's assumption of spherical symmetry and the model of Ney et al. and Gillett et al. in which the electron density is constant up to some latitude and then drops to zero. Thus our guess of $\epsilon \approx 1.0$ does not appear inconsistent with von Klüber, Ney et al., and Gillett et al.

F. Local Density and Scattering Enhancements

The large density enhancement on June 15 (Figures 10, 11, and 12) may be associated with an importance 2B flare which erupted an hour before the start of the Arecibo observations [Carrigan, 1973]. However, the flare occurred on the solar northern hemisphere (at N 15°, W 32°), while the pulsar was 5.6 $r_\odot$ southwest of the sun. Surprisingly, no scattering enhancement was observed concurrently.

The local density decrease observed on June 12 may correspond to a hole in the corona, a phenomenon which was occasionally observed with the Skylab coronagraph [MacQueen et al., 1974]. However, data on that day were taken for only the first half of the observing period due to a lightning bolt that struck the control room. It is possible that the day's observations are systematically biased due to the fact that data were taken only before transit. This possibility is considered highly unlikely, however, as all known sources of systematic error have been removed, and no such bias is observed on days with a full set of data. Although the rms scatter of the June 12 observations is no larger than that of June 11, the June 12 observations nevertheless represent a less reliable estimate of the typical properties of the corona because they do not reflect the averaging which occurs over a three-hour observing period. Hopefully, Skylab coronagraph observations will help to

determine whether the June 12 point represents a real variation in the density.

The only significant scattering enhancements occurred on June 12, whose data are slightly suspect, and June 14, the day of closest approach, when the earth-pulsar line-of-sight passed almost directly below the solar south pole. (See Figure 9.) At this time coronal scattering contributed 3.75 (± 1.0) ms of delay (referenced to a 100 MHz pulse).

V. DISCUSSION AND CONCLUSIONS

Coronal occultations of the Crab Nebula pulsar have now been observed over a substantial portion of the present solar cycle. It is sueful to compare the results of the four years.

A. Path-Integrated Electron Density

Figure 19 is a graphic demonstration of the changes in the corona that have accompanied the decline of solar activity from 1970 to 1973. The peak path-integrated density in 1969-70 was approximately twice its 1971 and 1973 values. But, four days before and after conjunction, the 1971 results show 50% more path-integrated density, and the 1973 results show 80% more than 1969-70. These results are consistent with a corona whose polar densities are decreasing as it becomes more concentrated toward the equator. It should be emphasized that the curves of Figure 19 are model-dependent. For example, if the 1971 value of ϵ was less than 1.0 or the 1973 value greater than 1.0, the two curves would tend toward each other at intermediate and large elongations. Or, if less weight is given to the 1973 June 15 enhancement in the least squares fits for that year, the peak of the 1973 curve declines. These changes do not alter the general conclusion that the corona has redistributed itself toward the equator since 1969-70.

B. Density Distribution

The parameters which characterize the overall density distribution of the corona as inferred from the Crab Pulsar occultation experiments in 1969, 1970, 1971, and 1973 are listed in Table 6. The equatorial density at 10 $r_\odot$ has remained relatively constant through the four years. The density averaged over all solar latitudes, ρ_o, declined significantly in 1971 and slightly more in 1973. The radial density gradient became less steep in 1971 and the trend may have continued into 1973. The corona had become highly concentrated toward the equator by 1971 and perhaps more so in 1973, while it appeared spherically symmetric in 1969 and 1970. When definitive data on the shape of the 1973 corona become available, less ambiguous conclusions can be drawn. However, it does seem reasonable to expect the trends which became evident in 1971 to continue into 1973. The Zürich smoothed sunspot number, a prime index of solar activity, declined from 66.7 in June 1971 to 38.6 in June 1973[3] [Solar-Geophysical Data, 1974].

C. Radio Scattering

In 1969 and 1970 the scattering delay in the arrival of a pulse referenced to 100 MHz exceeded 1 ms on every day for which the impact parameter was less than 12 $r_\odot$, the reached 34 (± 5.5) ms three hours after the eruption of a solar flare.

---

[3] The 1969 and 1970 occultations, whose results were so similar that they were combined, occurred when the Zürich smoothed sunspot number was 106.1 and 10.53, respectively, lending credence to its validity as a predictor of overall coronal structure.

In 1971 there was no measurable scattering delay except on one day, during which a large enhancement of electron density was also seen. At that time the scattering delay was 1.4 (± 0.5) ms at 100 MHz. In 1973 the scattering delay reached 3.75 (± 1.0) ms on the day of closest approach (June 14). No density enhancement was concurrently observed. On 12 June 1973 an enhancement of 2.0 ms was observed concurrently with a large drop in the density. If the coronal void on June 12 is real, our observations of increased scattering indicate that the matter in the void is highly inhomogeneous. This result is consistent with the work of Noci [1973] which, on the basis of an analysis of observations of coronal holes, suggests that they are the source of high velocity streams of solar wind. Further corroboration is provided by Pneuman [1973], who suggests that coronal holes are regions of open magnetic field lines which are likely to produce large density inhomogeneities.

No other significant scattering delays were observed in 1973. It is difficult to make any general conclusions regarding the general scattering properties of the corona in 1973 because the data which tend to show any scattering delay at all are sparse. Certainly the inhomogeneity of the corona has decreased markedly from its 1969 and 1970 levels. Our data indicate greater inhomogeneity than observed in 1971, but such conclusions may be based upon purely local coronal phenomena rather than any large-scale properties.

D. Local Phenomena

Density and scattering enhancements were observed on several days in 1969, 1970, 1971, and 1973. (See Table 7.) The most notable were an integrated-density enhancement of 10^{16} electrons cm^{-2} along with an increased scattering delay on 15 June 1969 associated with an active region, an integrated-density enhancement of 10^{16} electrons cm^{-2} on 9 and 10 June 1970 which was identified with a narrow coronal streamer at 20 $r_{\odot}$, an excess scattering delay of 31 ms (referenced to 100 MHz) which occurred three hours after the eruption of an importance 2 solar flare on 15 June 1970, and an integrated density enhancement of 10^{16} electrons cm^{-2} on 16 June 1971 tentatively identified with an active region on the back side of the sun. Our 1973 results show an integrated density enhancement of 10^{16} electrons cm^{-2} on June 15, one hour after the eruption of an importance 2 solar flare, and a possible coronal hole and scattering enhancement on June 12. It is clear that there is no simple relationship between density and scattering enhancements. There is also no simple relationship between the onset of a major solar flare and density or scattering enhancements: The 15 June 1970 flare apparently produced a scattering enhancement while the 15 June 1973 flare apparently produced a density enhancement.

ACKNOWLEDGMENTS

I especially wish to thank my co-investigators. I am very indebted to Dr. John M. Rankin, who has helped me at every stage of this work. This experiment would not have been possible without his advice and support. Dr. C. C. Counselman III of MIT taught me the difficult analysis techniques which were used here. Robert R. Payne's help with observation and analysis was indispensible.

Dr. James A. Van Allen is thanked for his advice and his enthusiastic encouragement of this project as well as his financial support of this thesis under NASA Grant NGL 16-001-002. His insistence upon a full examination of the implications of this work led to a much fuller understanding thereof, and, in the eyes of the author, a much better thesis.

The entire staff of Arecibo Observatory is thanked for their help. F. S. Harris, E. Castro, and T. Noya were particularly helpful. Arecibo Observatory is operated by Cornell University under a contract with the National Science Foundation.

Dr. J. D. Fix and Dr. S. D. Shawhan are thanked for their assistance in understanding difficult points of theory.

The digital antidisperser which was developed by Dr. V. Boriakoff of Cornell University was used to improve significantly the accuracy of this experiment.

I wish to thank Shirley Streeby and Donna Muller and John Birkbeck for doing such a fine job of typing this report and drawing the figures herein.

Finally, I am very indebted to my parents and to Vi Heffernan and John Bartholdi for their encouragement.

Table 1

Radiometer bandwidths and time constants.

Frequency MHz	Bandwidth KHz	Post Detection Time Constant ms
430.0	50	0.1
196.5	10	0.5
111.5	5	1.0
73.8	5	1.0

Table 2

Expected standard deviations in arrival times.

Frequency MHz	Expected σ Without Antidisperser μsec	Expected σ With Antidisperser μsec
430.0	120	35
196.5	286	82
111.5	552	100
73.8	3520	--

Table 3 Total observed dispersion.

Date = date of observation.

Solar impact parameter = closest approach of earth-pulsar line to center of sun, in solar radii.

Solar latitude of closest approach = the solar latitude of the point of closest approach to the sun of the earth-pulsar line.

Solar equatorial coordinates of earth = X, Y, and Z coordinates of the earth in solar equatorial coordinates (measured in solar radii).

Observed dispersion = the total (coronal + interstellar) dispersion parameter D. This parameter also corresponds to the total path integrated free-electron density from the pulsar to the earth. (1 sec MHz^2 = 0.743×10^{15} $e^- cm^{-2}$.)

Table 3

DATE	SOLAR IMPACT PARAMETER $R_\odot$	SOLAR LATITUDE OF CLOSEST APPROACH	SOLAR EQUATORIAL COORDINATES OF EARTH			OBSERVED DISPERSION SEC-MHZ^2
			X	Y	Z	
4/22/73	169.89	- 8°2	159.79	-147.09	-18.71	235734.8 ± 3.3
4/29/73	152.56	- 8°5	176.20	-127.32	-16.20	235740.8 ± 2.3
5/ 9/73	124.21	- 9°1	195.28	- 96.11	-12.23	235745.0 ± 4.5
5/12/73	115.07	- 9°3	199.90	- 86.26	-10.97	235741.1 ± 1.9
6/ 2/73	44.54	-13°4	217.61	- 12.80	- 1.63	235764.9 ± 2.2
6/ 4/73	37.42	-14°6	217.92	- 5.56	- 0.71	235769.5 ± 1.9
6/ 6/73	30.45	-16°4	217.99	1.52	0.19	235772.5 ± 4.3
6/ 8/73	23.23	-19°4	217.81	8.86	1.13	235771.4 ± 3.9
6/ 9/73	19.73	-21°6	217.63	12.44	1.58	235777.8 ± 1.7
6/10/73	16.27	-24°8	217.39	16.01	2.04	235779.7 ± 1.3
6/11/73	12.87	-29°7	217.10	19.60	2.49	235785.0 ± 4.7
6/12/73	9.62	-38°0	216.74	23.18	2.95	235776.0 ± 3.7
6/13/73	6.78	-53°8	216.32	26.74	3.40	235786.8 ± 2.1
6/14/73	5.04	-84°7	215.84	30.29	3.85	235793.6 ± 3.1
6/15/73	5.59	-54°8	215.30	33.88	4.31	235804.4 ± 2.0
6/16/73	7.93	-31°3	214.71	37.39	4.76	235793.7 ± 1.7
6/17/73	10.99	-19°5	214.05	40.92	5.21	235788.7 ± 1.6
6/18/73	14.35	-12°9	213.33	44.48	5.66	235788.3 ± 1.6

Table 3 (cont.)

DATE	SOLAR IMPACT PARAMETER $R_\odot$	SOLAR LATITUDE OF CLOSEST APPROACH	SOLAR EQUARORIAL COORDINATES OF EARTH			OBSERVED DISPERSION SEC-MHZ^2
			X	Y	Z	
6/19/73	17.76	- 8°9	212.56	47.97	6.10	235785.3 ± 1.8
6/20/73	21.26	- 6°2	211.73	51.48	6.55	235784.4 ± 1.7
6/21/73	24.76	- 4°2	210.84	54.94	6.99	235787.3 ± 1.7
6/23/73	31.82	- 1°7	208.89	61.85	7.87	235785. ± 1.6
6/25/73	38.90	0°0	206.70	68.70	8.74	235790.4 ± 1.7
6/27/73	45.94	+ 1°2	204.29	75.45	9.60	235786. ± 1.7
6/29/73	52.96	+ 2°0	201.65	82.15	10.45	235789.7 ± 1.8
7/ 1/73	59.92	+ 2°6	198.79	88.74	11.29	235788.6 ± 1.9
7/ 4/73	70.23	+ 3°4	194.10	98.43	12.52	235790.9 ± 1.1
7/ 7/73	80.40	+ 3°9	188.92	107.90	13.73	235793.9 ± 1.2
7/ 9/73	87.04	+ 4°2	185.22	114.03	14.51	235795.5 ± 1.3
7/11/73	93.60	+ 4°4	181.31	120.06	15.27	235800. ± 1.3
7/13/73	100.10	+ 4°7	177.18	125.98	16.03	235801.3 ± 1.8
7/15/73	106.44	+ 4°9	172.89	131.72	16.76	235804.7 ± 1.5

Table 4

Results of fits to a three-dimensional coronal model, with the flattening parameter fixed.

ϵ (fixed)	ρ_o (10^3 cm^{-3})	α	D_o s MHz^2	D_1 s MHz^2/day	D_2 (s MHz^2/day^2)	χ^2	ρ_{EQ} 10^3 cm^{-3}	ρ_{POLAR} 10^3 cm^{-3}
0	5.3	1.4	0	0.93	0.012	57	5.3	5.3
0.2	5.2	1.5	2.4	0.92	0.011	56	5.7	4.2
0.4	5.1	1.6	4.6	0.92	0.010	56	6.1	3.1
0.6	5.1	1.7	5.7	0.91	0.010	57	6.6	2.0
0.8	5.0	1.9	8.0	0.90	0.008	58	7.0	1.0
1.0	5.0	2.1	9.6	0.89	0.006	61	7.5	0.0
1.2*	5.0	2.3	10.5	0.88	0.005	64	8.0	0.0
1.4**	4.9	2.4	11.2	0.88	0.004	68	8.4	0.0

ϵ = flattening.

ρ_o = average coronal density at 10 $r_\odot$.

α = radial density gradient.

D_o, D_1, D_2 = interstellar dispersion and its first two time derivatives (an arbitrary constant has been subtracted from D_o).

χ^2 = sum of squares of postfit residuals, divided by standard deviation, with 27 degrees of freedom.

ρ_{EQ} = solar equatorial coronal density at 10 $r_\odot$.

ρ_{POLAR} = solar polar coronal density at 10 $r_\odot$.

* = electron density set to zero for all solar latitudes greater than 70.°5 North and South.

** = electron density set to zero for all latitudes greater than 64.°1 North and South.

The standard deviations are:

ρ_o = 300.

α = 0.2.

D_o = 1.6 for high values of ϵ; 6 for low values.

D_1 = 0.03.

D_2 = 0.003.

Table 5 Calculated interstellar baselines and dispersions, based upon the models of Table 4. 235735.0 sec MHz^2 have been arbitrarily subtracted from all dispersions and baselines.

Observed dispersion = the total (coronal + interstellar) dispersion parameter, D.

Calculated dispersion = the total dispersion parameter, D, as calculated by the best-fitting models for ϵ = 0.4, 0.6, 0.8, 1.0, 1.2, and 1.4.

Interstellar baseline = the interstellar component of the total dispersion parameter, as calculated by the best-fitting models for ϵ = 0.4, 0.6, 0.8, 1.0, 1.2, and 1.4.

Table 5

DATE	OBSERVED DISPERSION SEC-MHZ^2	FOR ϵ = 0.4 CALCULATED DISPERSION SEC-MHZ^2	FOR ϵ = 0.4 INTERSTELLAR BASELINE SEC-MHZ^2	FOR ϵ = 0.6 CALCULATED DISPERSION SEC-MHZ^2	FOR ϵ = 0.6 INTERSTELLAR BASELINE SEC-MHZ^2	FOR ϵ = 0.8 CALCULATED DISPERSION SEC-MHZ^2	FOR ϵ = 0.8 INTERSTELLAR BASELINE SEC-MHZ^2	FOR ϵ = 1.0 CALCULATED DISPERSION SEC-MHZ^2	FOR ϵ = 1.0 INTERSTELLAR BASELINE SEC-MHZ^2	FOR ϵ = 1.2 CALCULATED DISPERSION SEC-MHZ^2	FOR ϵ = 1.2 INTERSTELLAR BASELINE SEC-MHZ^2	FOR ϵ = 1.4 CALCULATED DISPERSION SEC-MHZ^2	FOR ϵ = 1.4 INTERSTELLAR BASELINE SEC-MHZ^2
4/22/73	-0.2 ± 3.3	-0.2	-2.6	-0.3	-2.2	-0.9	-1.9	-1.4	-2.0	-1.8	-2.2	-2.0	-2.3
4/29/73	5.8 ± 2.3	3.0	0.3	3.0	0.9	2.9	1.7	2.8	2.1	2.7	2.2	2.7	2.3
5/ 9/73	10.0 ± 4.5	8.6	5.3	8.7	6.1	9.1	7.5	9.5	[illegible]	9.7	9.0	9.9	9.3
5/12/73	6.1 ± 1.9	10.6	6.9	10.7	7.8	11.1	9.4	11.6	10.5	11.9	11.1	12.1	11.5
6/ 2/73	29.9 ± 2.2	29.2	21.2	29.2	22.3	29.5	24.5	29.8	26.2	30.0	27.1	30.2	27.8
6/ 4/73	34.5 ± 1.9	31.9	22.8	31.9	23.9	32.0	26.2	32.2	27.9	32.3	28.8	32.5	29.5
6/ 6/73	37.5 ± 4.3	34.9	24.5	34.9	25.5	34.9	27.8	35.0	29.5	35.0	30.4	35.1	31.1
6/ 8/73	36.[illegible] ± 3.9	38.9	26.2	38.[illegible]	27.2	38.6	29.5	38.5	31.2	38.5	32.2	38.5	32.8
6/ 9/73	42.8 ± 1.7	41.2	27.0	41.1	28.1	40.9	30.3	40.8	32.1	40.7	33.0	40.6	33.7
6/10/73	44.[illegible] ± 1.3	44.0	27.9	43.9	28.9	43.7	31.2	43.5	32.9	43.4	33.8	43.3	34.5
6/11/73	50.[illegible] ± 4.7	47.4	28.7	47.4	29.8	47.2	32.1	47.0	33.8	47.0	34.7	46.9	35.4
6/12/73	41.[illegible] ± 3.7	51.8	29.6	51.7	30.7	51.6	33.0	51.6	34.6	51.5	35.6	51.5	36.3
6/13/73	[illegible] ± 2.1	56.9	30.5	56.4	31.6	56.3	33.8	56.1	35.5	55.7	36.4	55.1	37.1
6/14/73	[illegible] ± 3.1	61.0	31.4	59.7	32.5	58.6	34.7	57.2	36.4	56.0	37.3	55.3	38.0
6/15/73	6[illegible] ± 2.0	62.3	32.3	62.1	33.4	62.3	35.6	62.5	37.3	62.3	38.2	61.9	38.9
6/16/73	[illegible]9.7 ± 1.7	59.1	33.2	59.6	34.3	60.2	36.5	60.8	38.2	61.3	39.1	61.8	39.7
6/17/73	53.7 ± 1.6	55.6	34.2	56.0	35.2	56.1	37.4	56.3	39.0	56.4	40.0	56.6	40.6
6/18/73	[illegible]3 ± 1.6	53.2	35.1	53.3	36.2	53.3	38.4	53.1	40.0	53.1	40.9	53.1	41.5
6/19/73	[illegible] ± 1.8	51.7	36.1	51.8	37.[illegible]	51.6	39.3	51.4	40.9	51.2	41.8	51.2	42.4
6/20/73	49.4 ± 1.7	50.8	37.0	50.9	38.1	50.6	40.2	50.4	41.8	50.3	42.7	50.2	43.3
6/21/73	52.[illegible] ± 1.7	50.4	38.0	50.4	39.0	50.2	41.2	50.0	42.7	49.9	43.6	49.8	44.2
6/23/73	50.0 ± 1.6	50.3	40.0	50.2	41.0	50.1	43.1	50.0	44.6	50.0	45.4	49.9	46.0
6/25/73	55.4 ± 1.7	50.9	42.0	50.8	43.0	50.8	45.0	50.8	46.5	50.8	47.3	50.8	47.8
6/27/73	51.0 ± 1.7	51.9	44.0	51.8	45.0	51.9	47.0	51.9	48.4	52.0	49.1	52.0	49.7
6/29/73	54.7 ± 1.8	53.1	46.1	53.1	47.1	53.2	49.0	53.3	50.5	53.4	51.0	53.5	51.5
7/ 1/73	53.6 ± 1.9	54.6	48.3	54.6	49.2	54.7	51.0	54.9	52.3	54.9	53.0	55.0	53.4
7/ 4/73	55.9 ± 1.1	57.1	51.5	57.1	52.5	57.3	54.1	57.4	55.3	57.5	55.9	57.5	56.3
7/ 7/73	58.9 ± 1.2	59.9	55.0	59.9	55.8	60.0	57.3	60.1	58.3	60.2	58.8	[illegible].2	59.2
7/ 9/73	60.5 ± 1.3	61.9	57.2	61.9	58.0	61.9	59.5	62.0	60.4	62.0	60.8	62.0	61.1
7/11/73	65.0 ± 1.3	63.9	59.5	63.9	60.4	63.9	61.6	63.9	62.4	63.9	62.8	63.9	63.1
7/13/73	66.3 ± 1.8	66.1	61.9	66.1	62.7	66.0	63.9	65.9	64.6	65.8	64.9	65.8	65.1
7/15/73	69.[illegible] ± [illegible].5	68.2	64.3	68.2	65.1	68.1	66.1	67.9	66.7	67.8	66.9	67.7	67.0

Table 6

A summary of the parameters which characterized the overall density distribution of the corona in 1969, 1970, 1971, and 1973.

Year	ρ_{EQ} (10^3 cm^{-3})	ρ_o (10^3 cm^{-3})	α	ϵ
1969-70	7.0	7.0	2.9	~ 0
1971	6.2-8.4	5.2-5.6	≥ 2.0	≥ 0.4
1973	6.6-7.5	5.0-5.3	≥ 2.0	≥ 0.6

Table 7

A summary of notable local variations in integrated density and scattering.

Year	Density Variation 10^{16} e$^-$ cm^{-2}	Scattering Enhancement	Associated Phenomenon
1969 June 15	+ 1	Yes	Active region
1970 June 9-10	+ 1	No	Coronal streamer at 20 $r_\odot$
1970 June 15	--	Yes	Solar flare
1971 June 16	+ 1	Yes	Active region (?)
1973 June 12	- 1	Yes	Coronal void (?)
1973 June 15	+ 1	No	Solar flare (?)

LIST OF REFERENCES

Boriakoff, V. 1973, Ph.D. Thesis, Cornell University.

Campbell, D. B. and Muhleman, D. O. 1969, J. Geophys. Res., 74, 1138.

Carrigan, A. L., ed. 1973, Geophysics and Space Data Bulletin, Air Force Cambridge Research Laboratories Special Report No. 166, AFCRL-TR-73-0514.

Counselman, C. C. III and Rankin, J. M. 1971, Ap. J., 166, 513.

Counselman, C. C. III and Rankin, J. M. 1972, Ap. J., 175, 843.

Counselman, C. C. III and Rankin, J. M. 1973, Ap. J., 185, 357.

Counselman, C. C. III and Shapiro, I. I. 1968, Science, 162, 353.

Cox, A. N. and Liebenberg, D. H. 1973, Sky and Telescope, 46, 222.

Erickson, W. C. 1964, Ap. J., 139, 1290.

Garriott, O. K., Smith, F. L. III, and Yuen, P. C. 1965, Planetary Space Sci., 13, 829.

Gillett, F. C., Stein, W. A., and Ney, E. P. 1964, Ap. J., 140, 292.

Hulst, H. C. van de. 1950, Bull. Astron. Inst. Neth., 11, 135.

Hundhausen, A. J. 1972a, Coronal Expansion and Solar Wind (New York: Springer-Verlag), 16-19.

Hundhausen, A. J. 1972b, in Physics of the Solar System, NASA SP-300, ed. by S. I. Rasool (Washington: U. S. Government Printing Office).

Klüber, H. von. 1958, M.N.R.A.S., 118, 201.

Koehler, R. L. 1968, J. Geophys. Res., 73, 4883.

MacQueen, R. M., Eddy, J. A., Gosling, J. T., Hildner, E., Munro, R. H., Newkirk, G. A. Jr., Poland, A. I., and Ross, C. L. 1974, Ap. J. (Letters), 187, 185.

Newkirk, G. Jr. 1967, Ann. Rev. Astr. and Ap., 5, 213.

Ney, E. P., Huch, W. F., Kellogg, P. J., Stein, W., and Gillett, F. 1961, Ap. J., 133, 616.

Noci, G. 1973, Solar Phys., 28, 403.

Pneuman, G. W. 1973, Solar Phys., 28, 247.

Rankin, J. M. 1970, Ph.D. Thesis, University of Iowa.

Rankin, J. M. and Counselman, C. C. III 1973, Ap. J., 181, 875.

Rankin, J. M., Payne, R. R., and Campbell, D. B. 1974, Ap. J. (Letters), 193, L71.

Solar-Geophysical Data 1974, IER-FB355, Part I (Boulder, Colorado: U. S. Department of Commerce).

Staff, Center for Radar Astronomy 1966, J. Geophys. Res., 71, 3325.

LIST OF FIGURES

Figure 8 The total (coronal + interstellar) observed dispersion, D. (1 sec MHz^2 = 0.743 × 10^{15} e^- cm^{-2}.)

Figure 9 The scattering parameter, S.

Figure 10 The measured coronal dispersion and the best model of dispersion versus time for ϵ = 0.6.

Figure 11 The measured coronal dispersion and the best model of dispersion versus time for ϵ = 1.0.

Figure 12 The measured coronal dispersion and the best model of dispersion versus time for ϵ = 1.4.

Figure 13 Contours of equal path-integrated coronal electron density, predicted by the best fitting model for ϵ = 0.6, as viewed from the earth in mid-June. The position of the pulsar behind the corona is shown at transit for each date in mid-June.

Figure 14 Contours of equal path-integrated coronal electron density, predicted by the best fitting model for ϵ = 1.0, as viewed from the earth in mid-June. The position of the pulsar behind the corona is shown at transit for each date in mid-June.

Figure 15 Contours of equal path-integrated coronal electron density, predicted by the best-fitting model for ϵ = 1.4, as viewed from the earth in mid-June. The position of the pulsar behind the corona is shown at transit for each date in mid-June.

Figure 16 K-coronal intensity isophotes, predicted by the best fitting model for $\epsilon = 0.6$, as viewed from the earth in mid-June. Successive contours differ in intensity by a factor of 5. The position of the pulsar behind the corona is shown at transit for each date in mid-June.

Figure 17 K-coronal intensity isophotes, predicted by the best fitting model for $\epsilon = 1.0$, as viewed from the earth in mid-June. Successive contours differ in intensity by a factor of 5. The position of the pulsar behind the corona is shown at transit for each date in mid-June.

Figure 18 K-coronal intensity isophotes, predicted by the best fitting model for $\epsilon = 1.4$, as viewed from the earth in mid-June. Successive contours differ in intensity by a factor of 5. The position of the pulsar behind the corona is shown at transit for each date in mid-June.

Figure 19 A comparison of certain best-fitting models of dispersion versus time in 1969-1970 (spherically symmetric); 1971 (no electrons above the poles); and 1973 (also no electrons above the poles). The curves for each successive year have been skewed by a quarter day in order that the sun-earth-pulsar geometry (rather than the date) is aligned in all three. (The 1969-1970 and 1971 curves are from Counselman and Rankin [1972] and Counselman and Rankin [1973], respectively.)

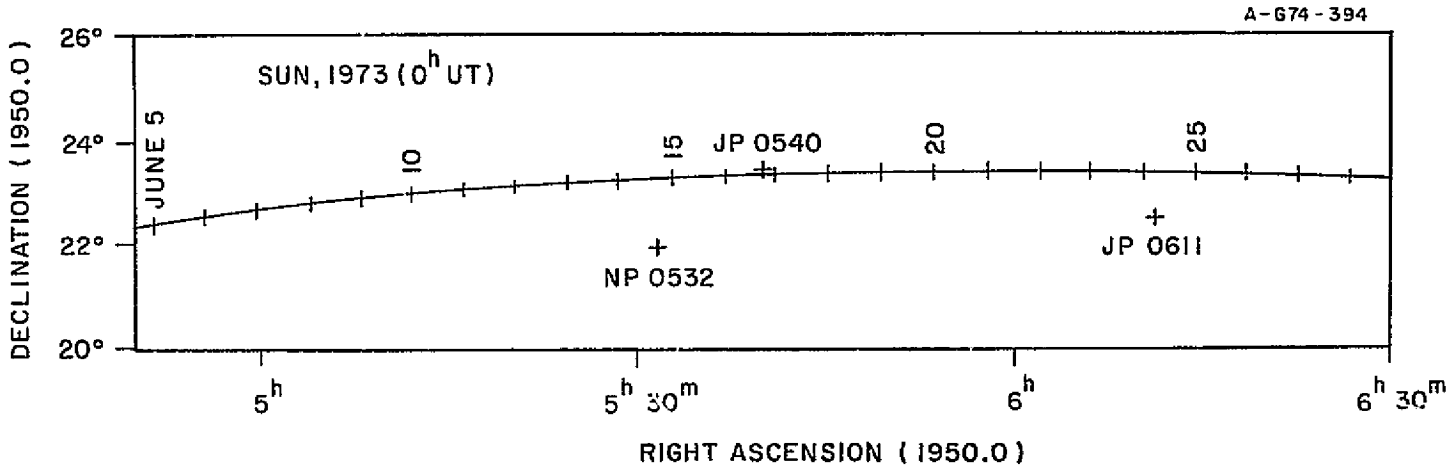
A-674-394
SUN, 1973 (0h UT)
JUNE 5
10
15
20
25
JP 0540
NP 0532
JP 0611
26°
24°
22°
20°
DECLINATION (1950.0)
5h
5h 30m
6h
6h 30m
RIGHT ASCENSION (1950.0)

Figure 1

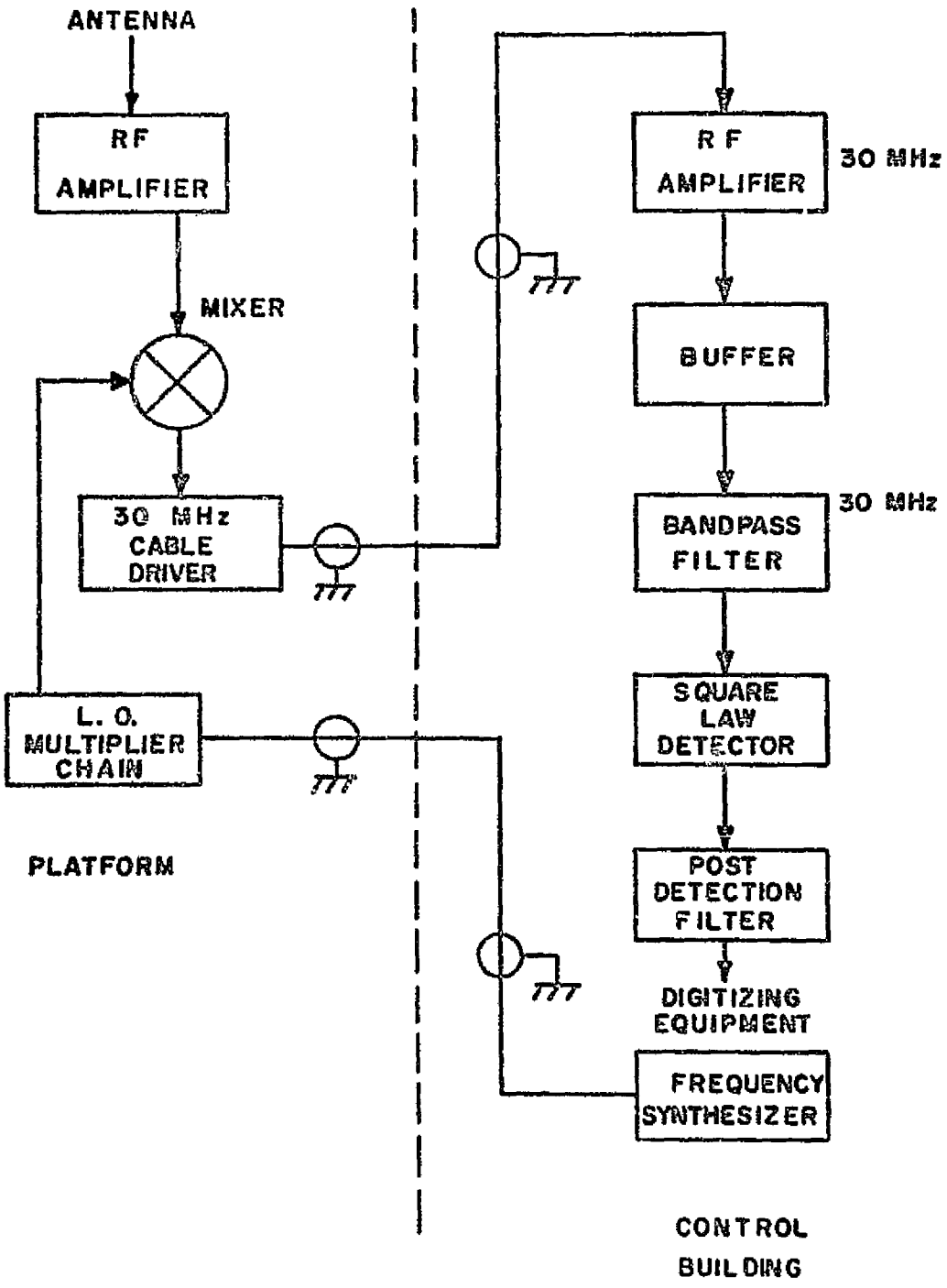
ANTENNA
RF AMPLIFIER
MIXER
30 MHz CABLE DRIVER
L. O. MULTIPLIER CHAIN
PLATFORM
R F AMPLIFIER
30 MHz
BUFFER
BANDPASS FILTER
30 MHz
SQUARE LAW DETECTOR
POST DETECTION FILTER
DIGITIZING EQUIPMENT
FREQUENCY SYNTHESIZER
CONTROL BUILDING

Figure 2

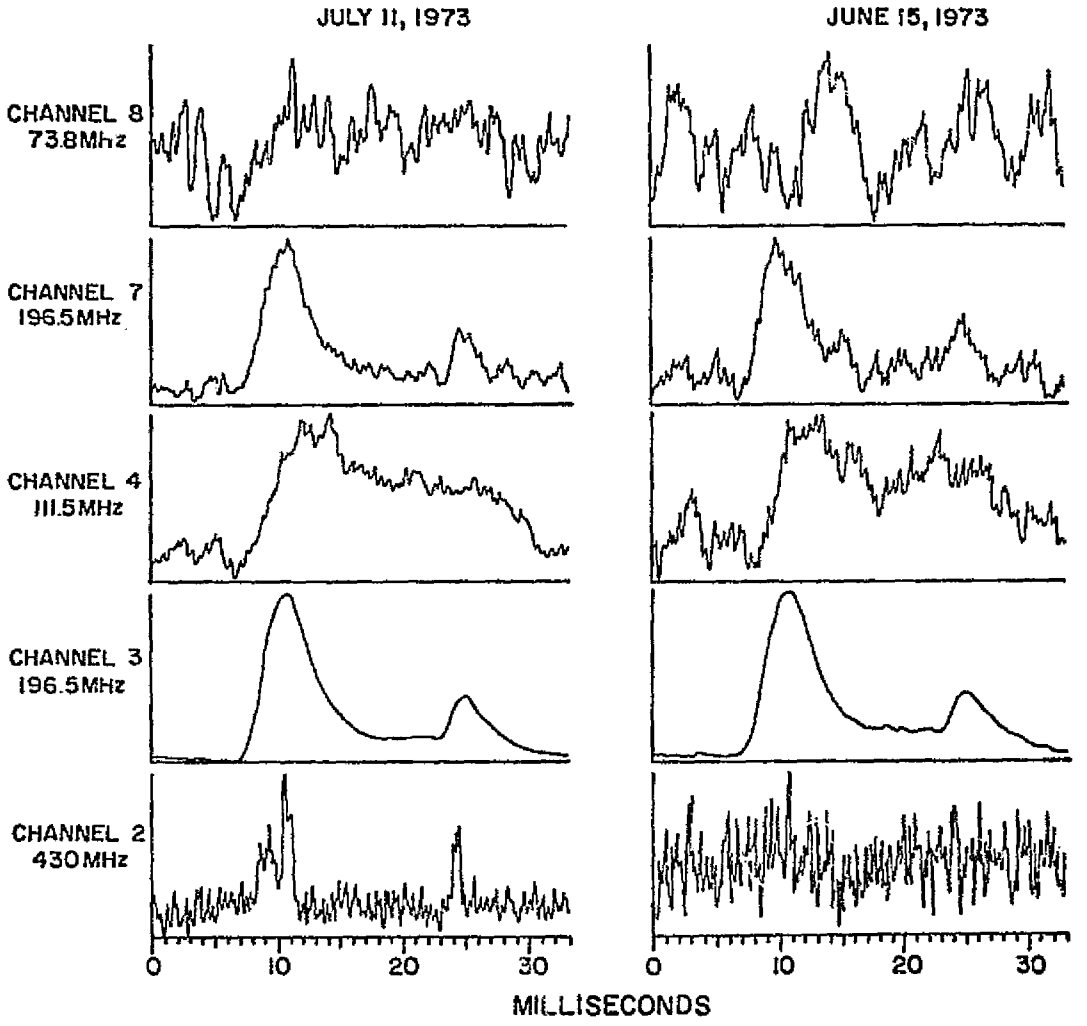
JULY 11, 1973
JUNE 15, 1973
CHANNEL 8
73.8MHz
CHANNEL 7
196.5MHz
CHANNEL 4
111.5MHz
CHANNEL 3
196.5MHz
CHANNEL 2
430MHz
0
10
20
30
0
10
20
30
MILLISECONDS

Figure 3

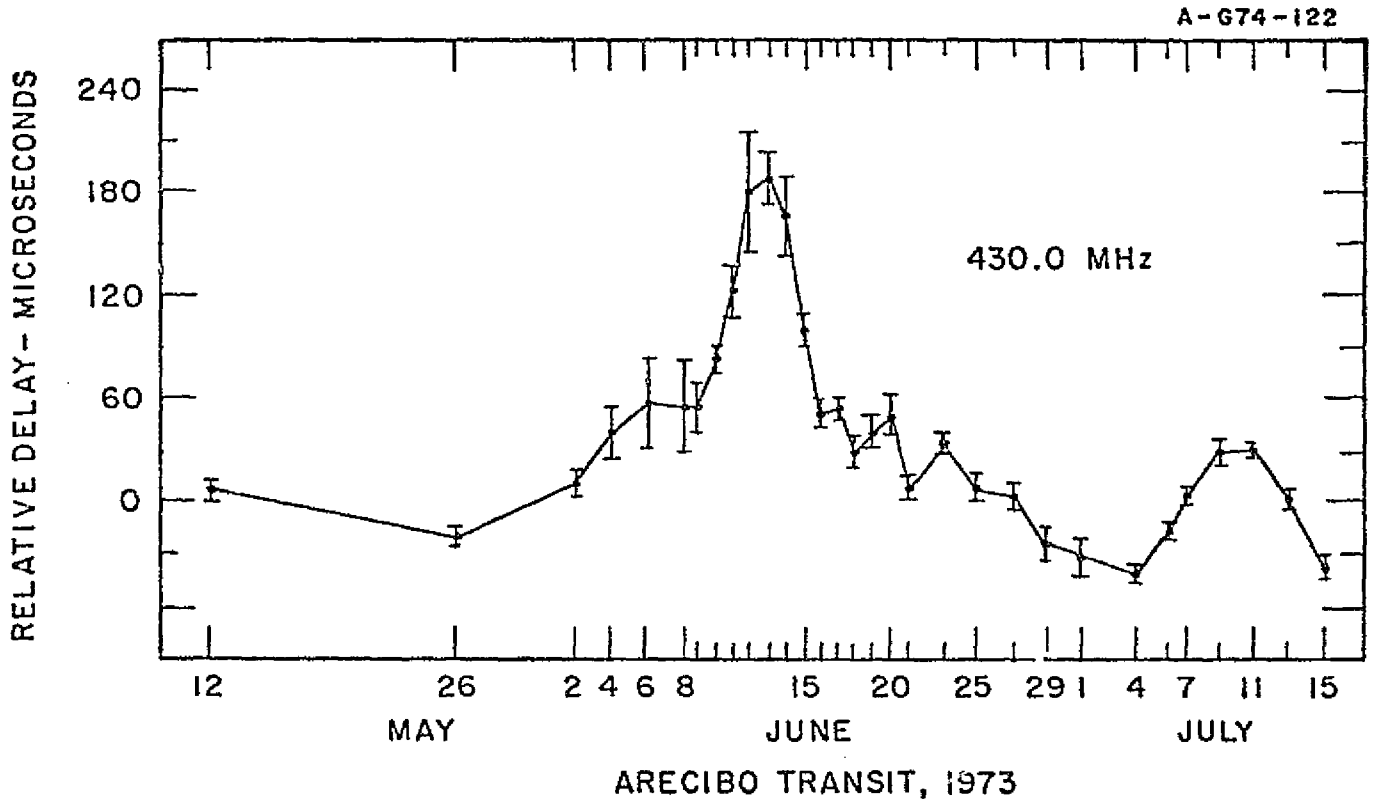
A-G74-122
RELATIVE DELAY- MICROSECONDS
240
180
120
60
0
430.0 MHz
12
26
2 4 6 8
15
20
25
29 1
4
7
11
15
MAY
JUNE
JULY
ARECIBO TRANSIT, 1973

Figure 4

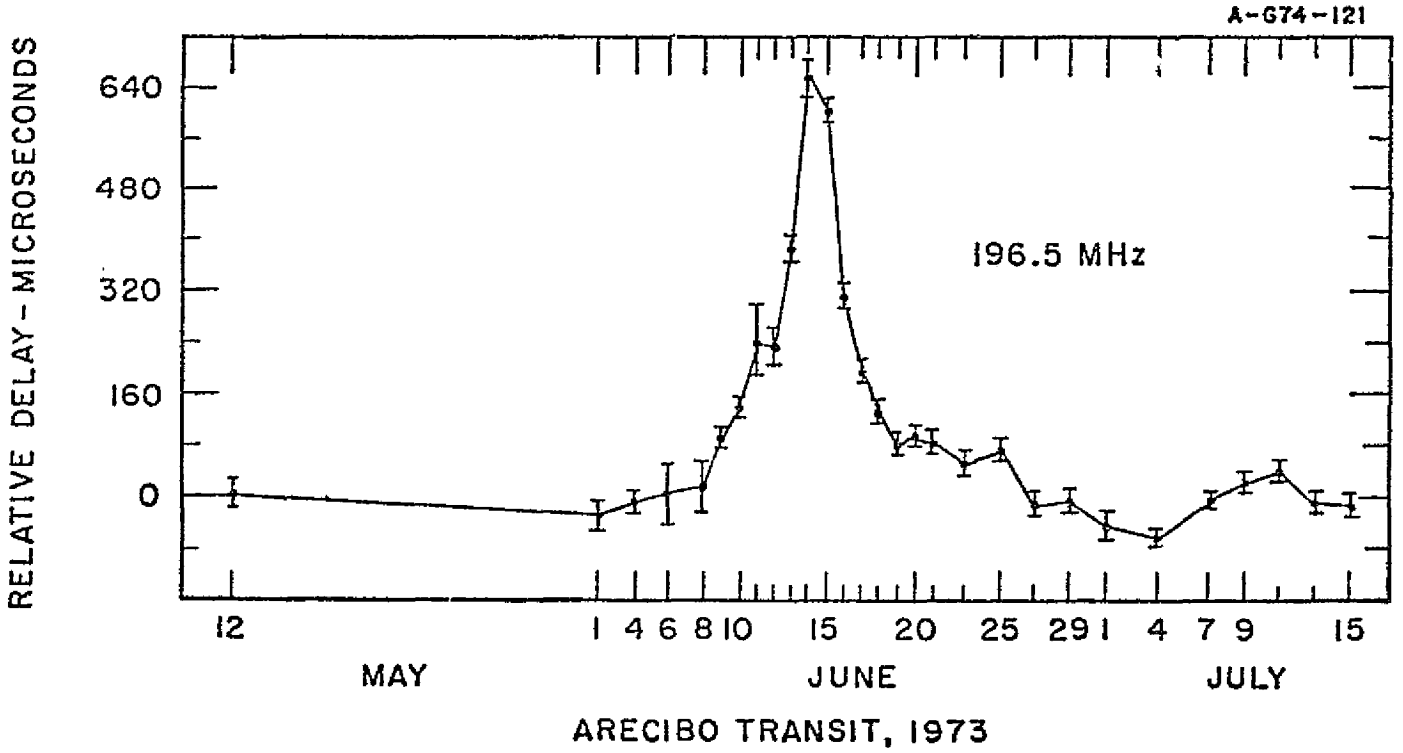
A-G74-121
RELATIVE DELAY - MICROSECONDS
640
480
320
160
0
196.5 MHz
12
1 4 6 8 10 15 20 25 29 1 4 7 9 15
MAY
JUNE
JULY
ARECIBO TRANSIT, 1973

Figure 5

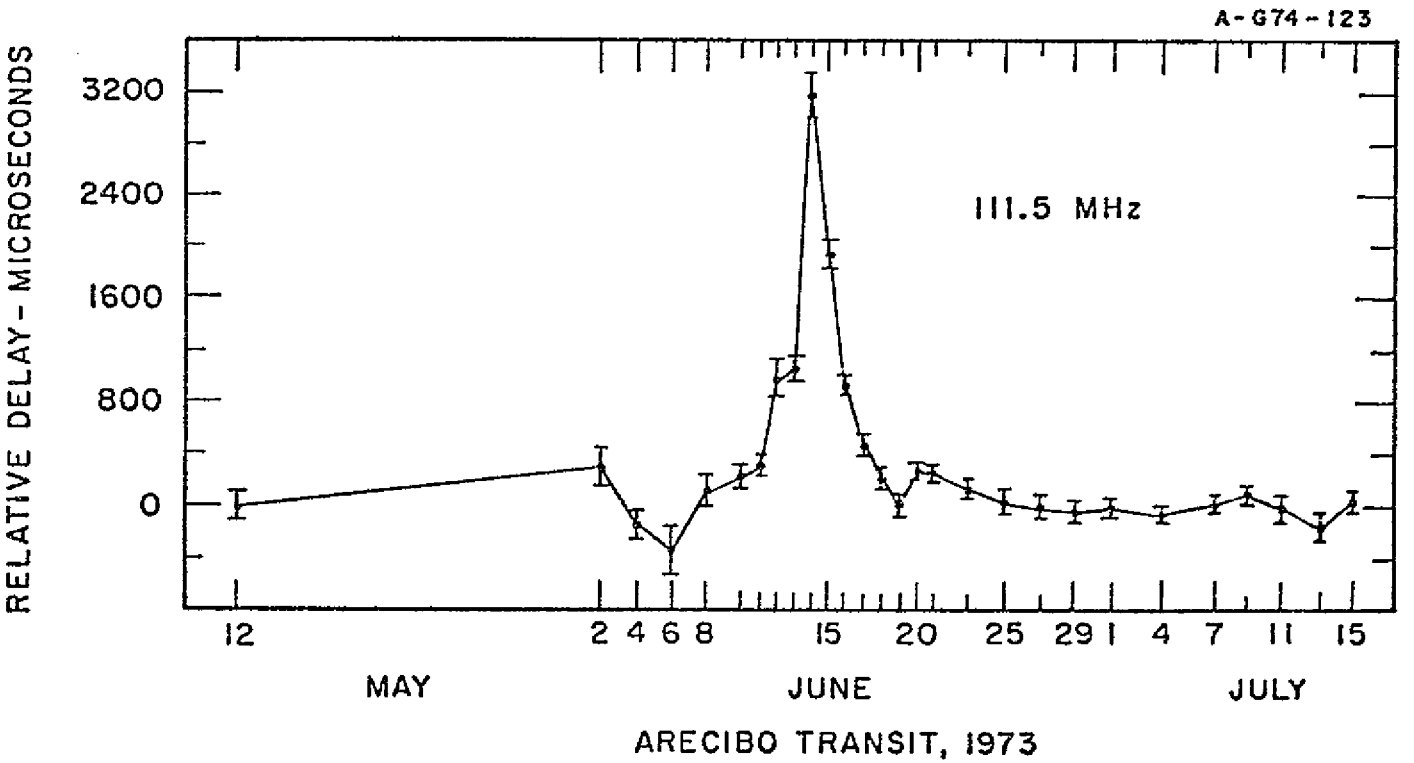
A-G74-123
RELATIVE DELAY - MICROSECONDS
3200
2400
1600
800
0
111.5 MHz
12
2 4 6 8
15
20
25
29
1 4 7 11 15
MAY
JUNE
JULY
ARECIBO TRANSIT, 1973

Figure 6

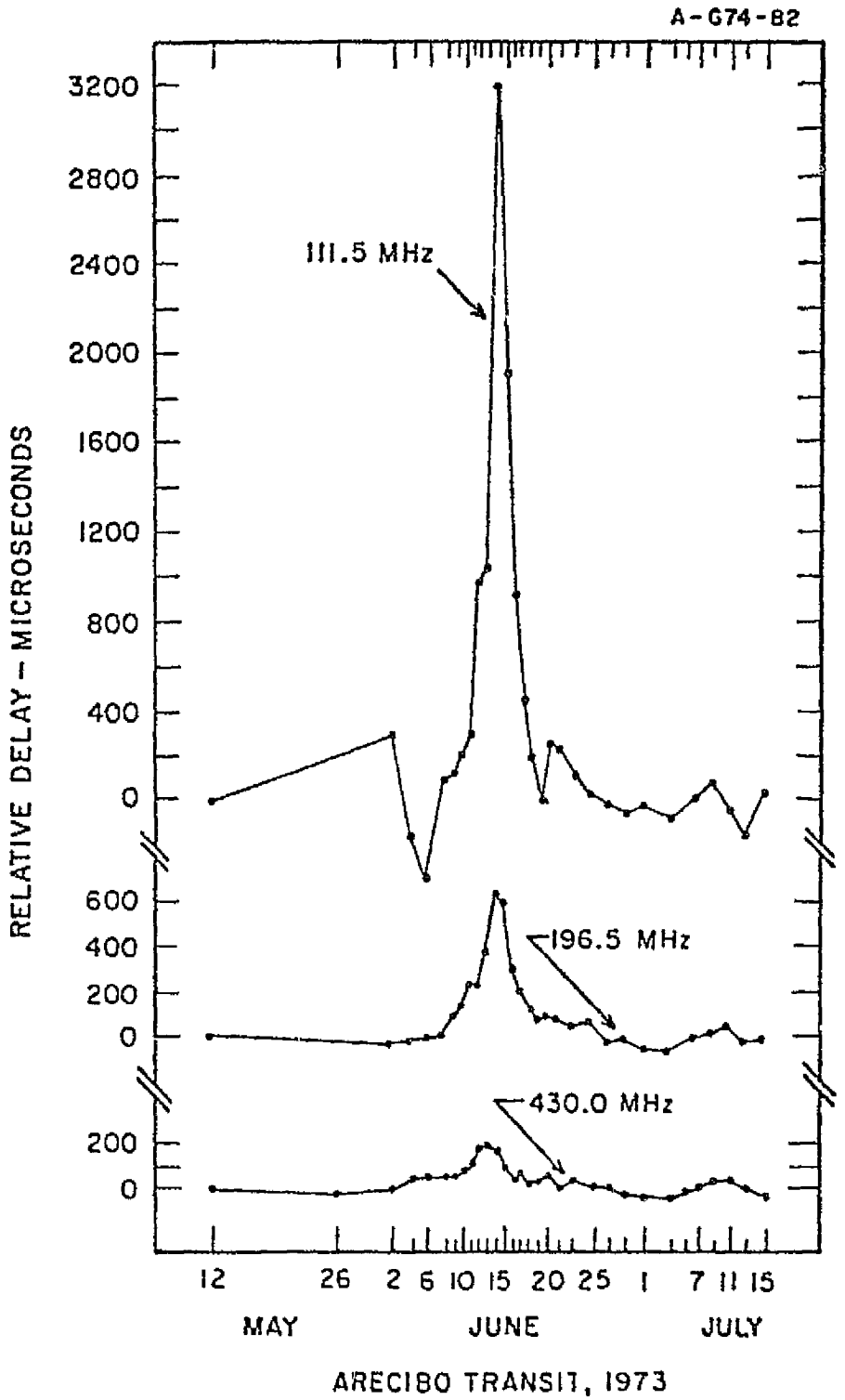
A-G74-82
RELATIVE DELAY - MICROSECONDS
3200
2800
2400
2000
1600
1200
800
400
0
111.5 MHz
600
400
200
0
196.5 MHz
200
0
430.0 MHz
12
26
2 6 10 15 20 25
1 7 11 15
MAY
JUNE
JULY
ARECIBO TRANSIT, 1973

Figure 7

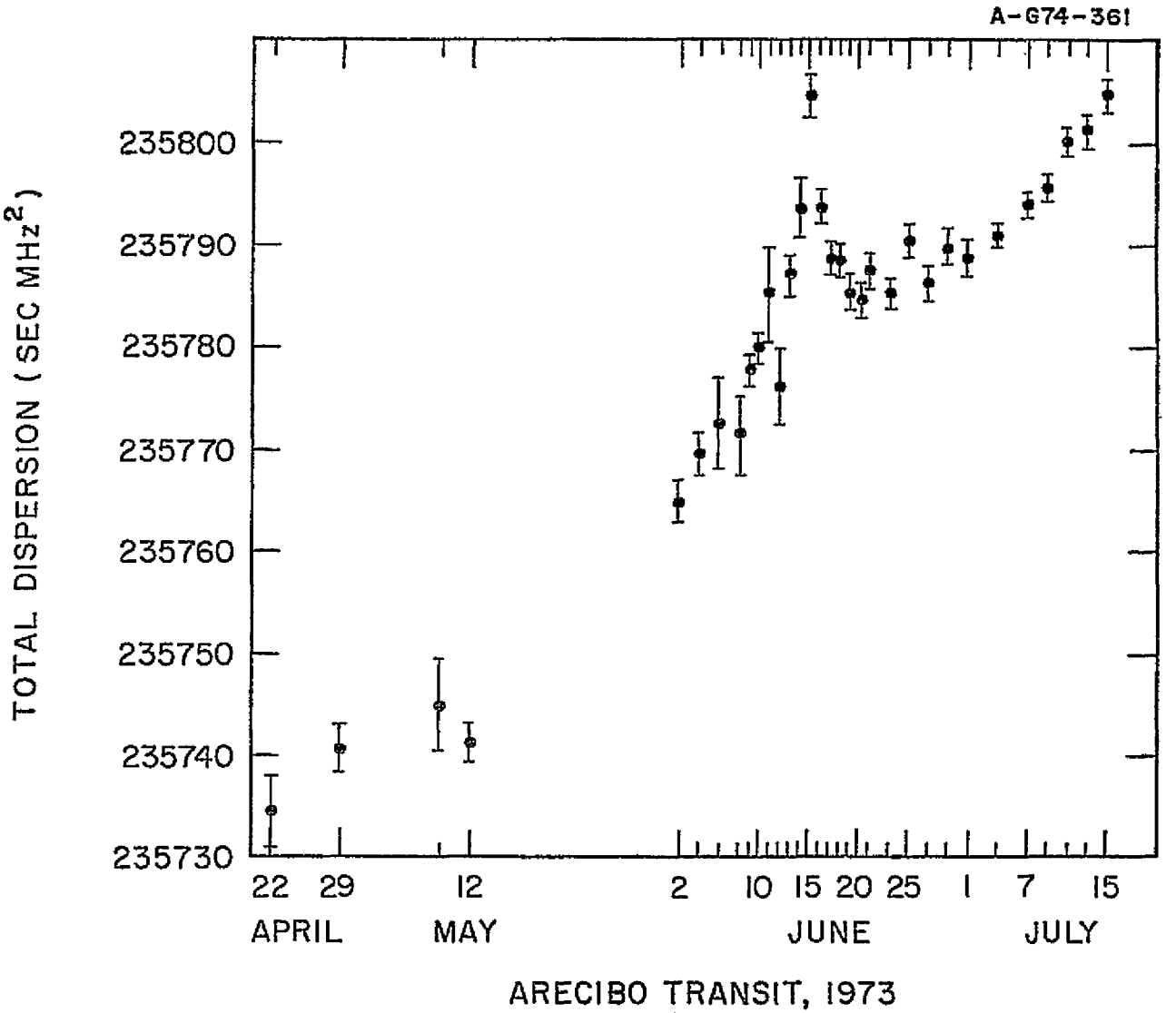
A-G74-361
TOTAL DISPERSION (SEC MHz^2)
235800
235790
235780
235770
235760
235750
235740
235730
22
29
12
2
10
15
20
25
1
7
15
APRIL
MAY
JUNE
JULY
ARECIBO TRANSIT, 1973

Figure 8

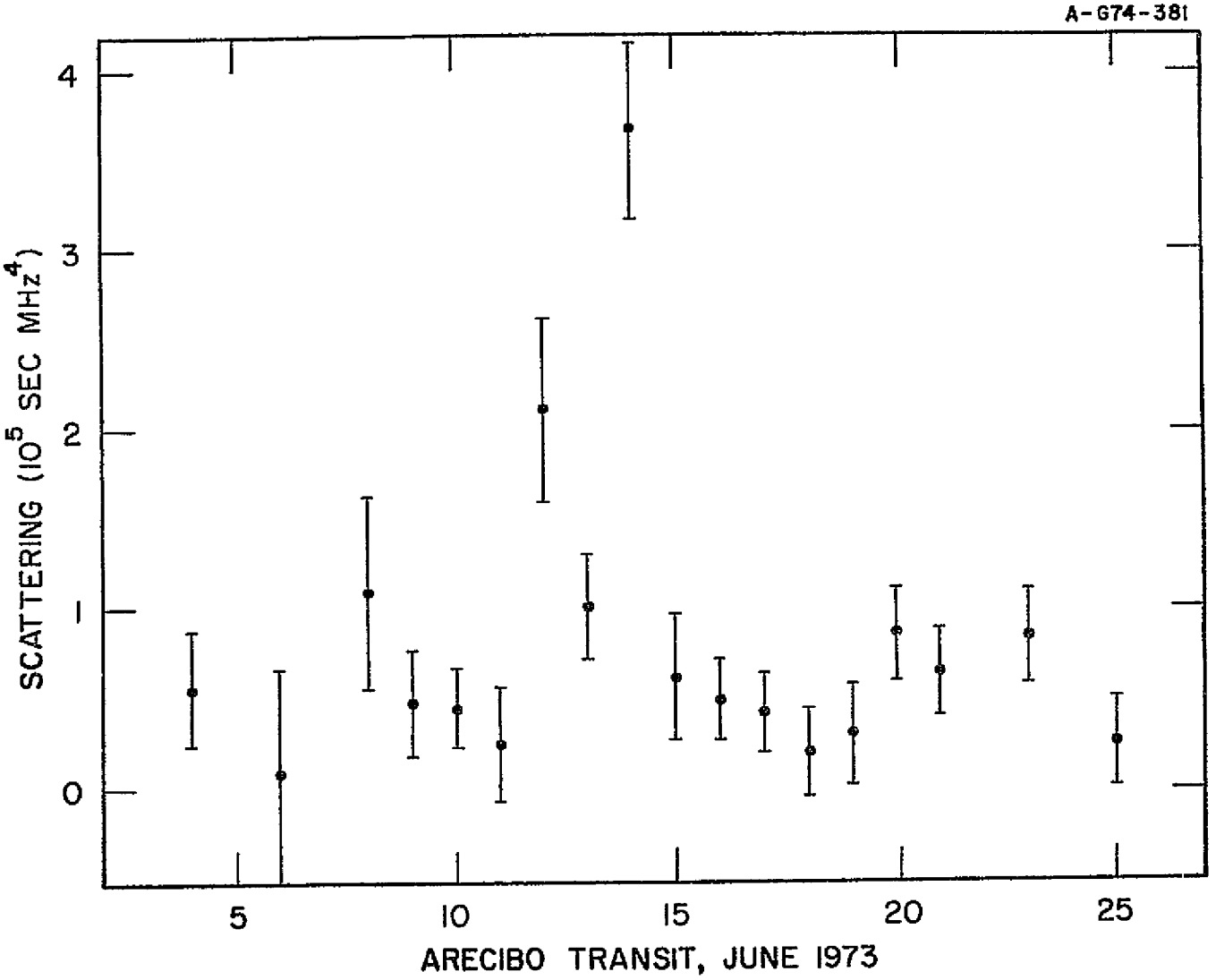
A-G74-381
SCATTERING (10^5 SEC MHz^4)
0
1
2
3
4
5
10
15
20
25
ARECIBO TRANSIT, JUNE 1973

Figure 9

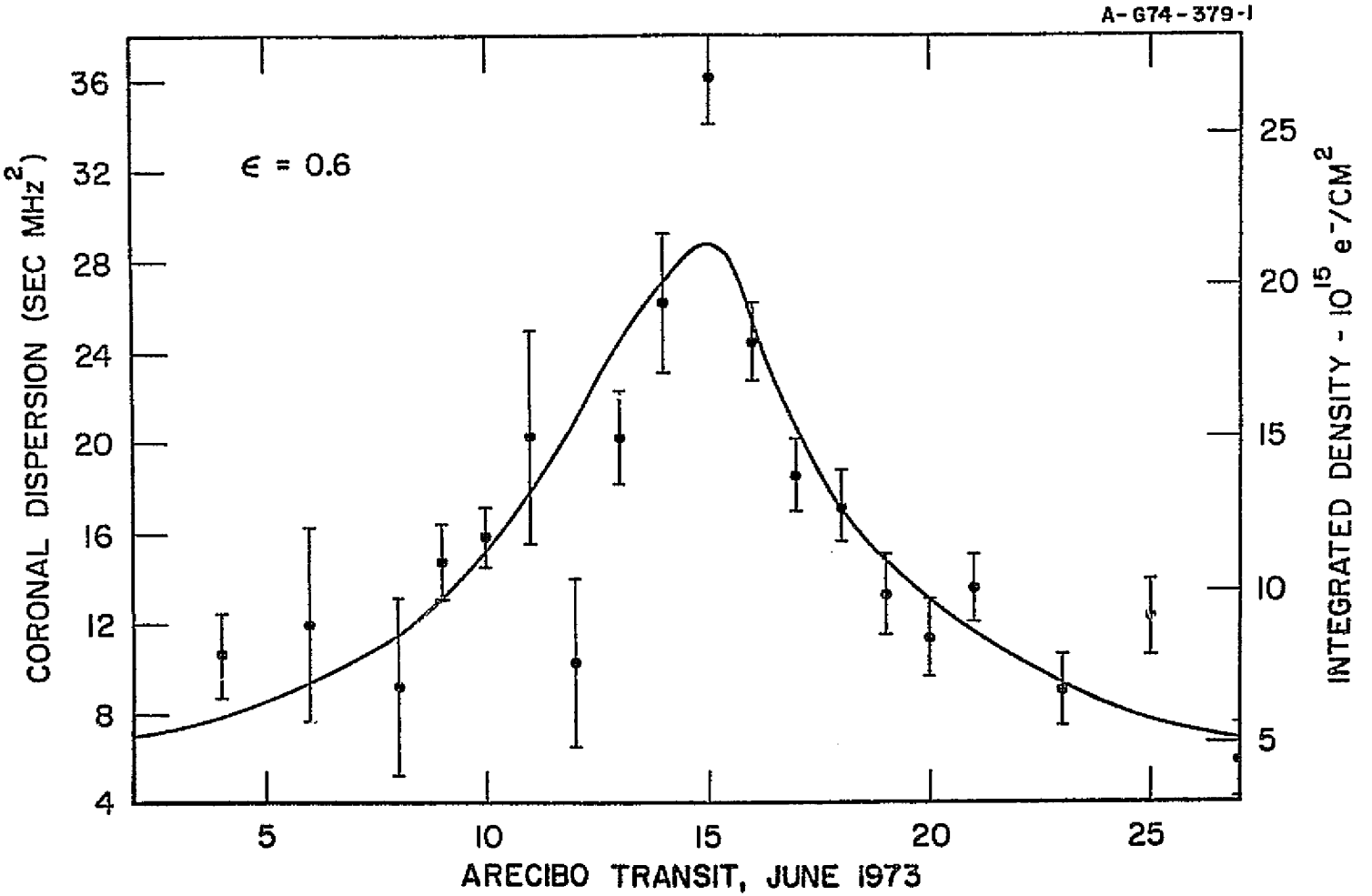
A-674-379-1
ϵ = 0.6
CORONAL DISPERSION (SEC MHz^2)
INTEGRATED DENSITY - 10^{15} e$^-$/CM^2
36
32
28
24
20
16
12
8
4
25
20
15
10
5
5
10
15
20
25
ARECIBO TRANSIT, JUNE 1973

Figure 10

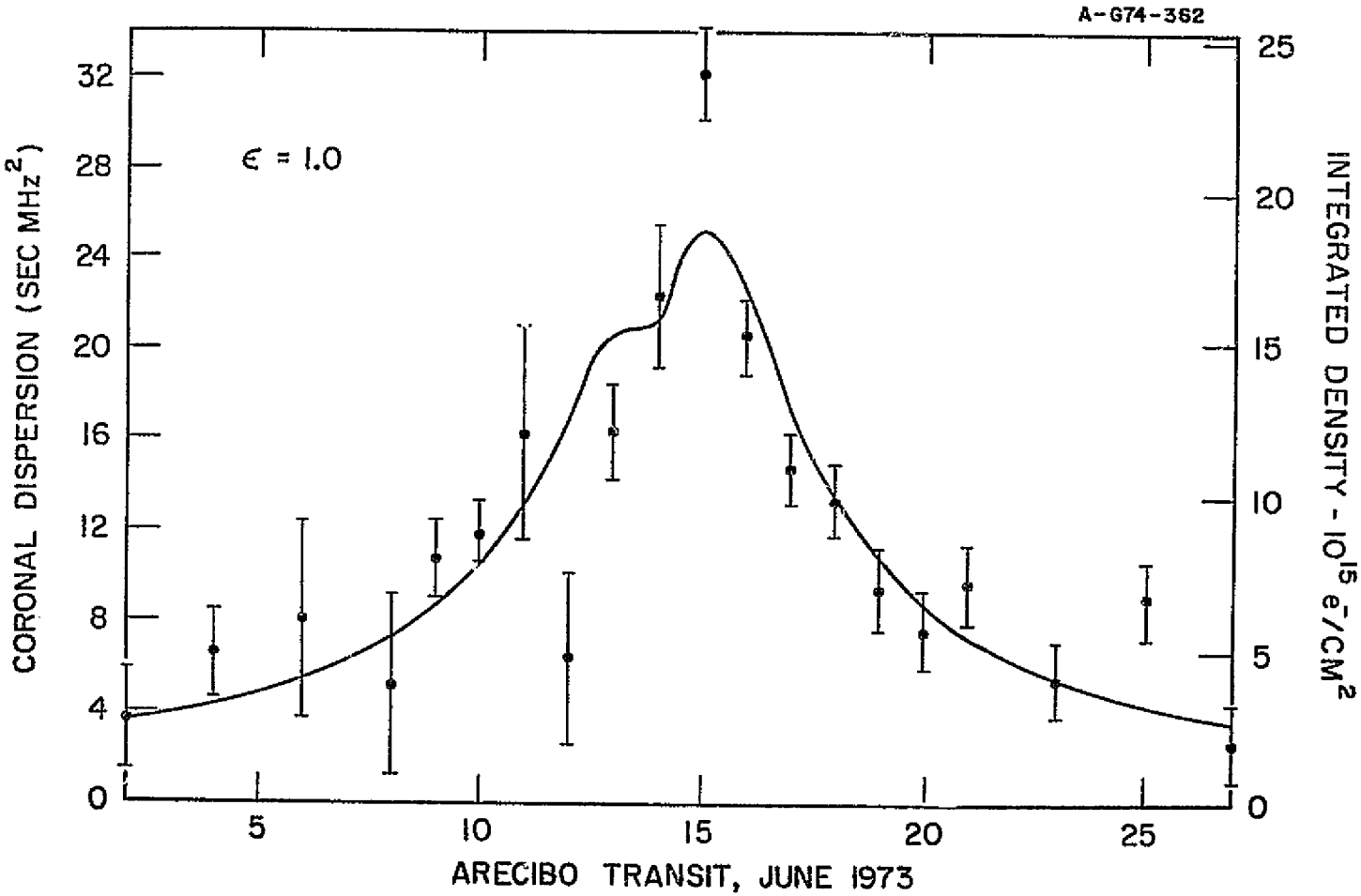
A-G74-362
ϵ = 1.0
CORONAL DISPERSION (SEC MHz²)
INTEGRATED DENSITY - 10¹⁵ e⁻/CM²
ARECIBO TRANSIT, JUNE 1973
0
4
8
12
16
20
24
28
32
0
5
10
15
20
25
5
10
15
20
25

Figure 11

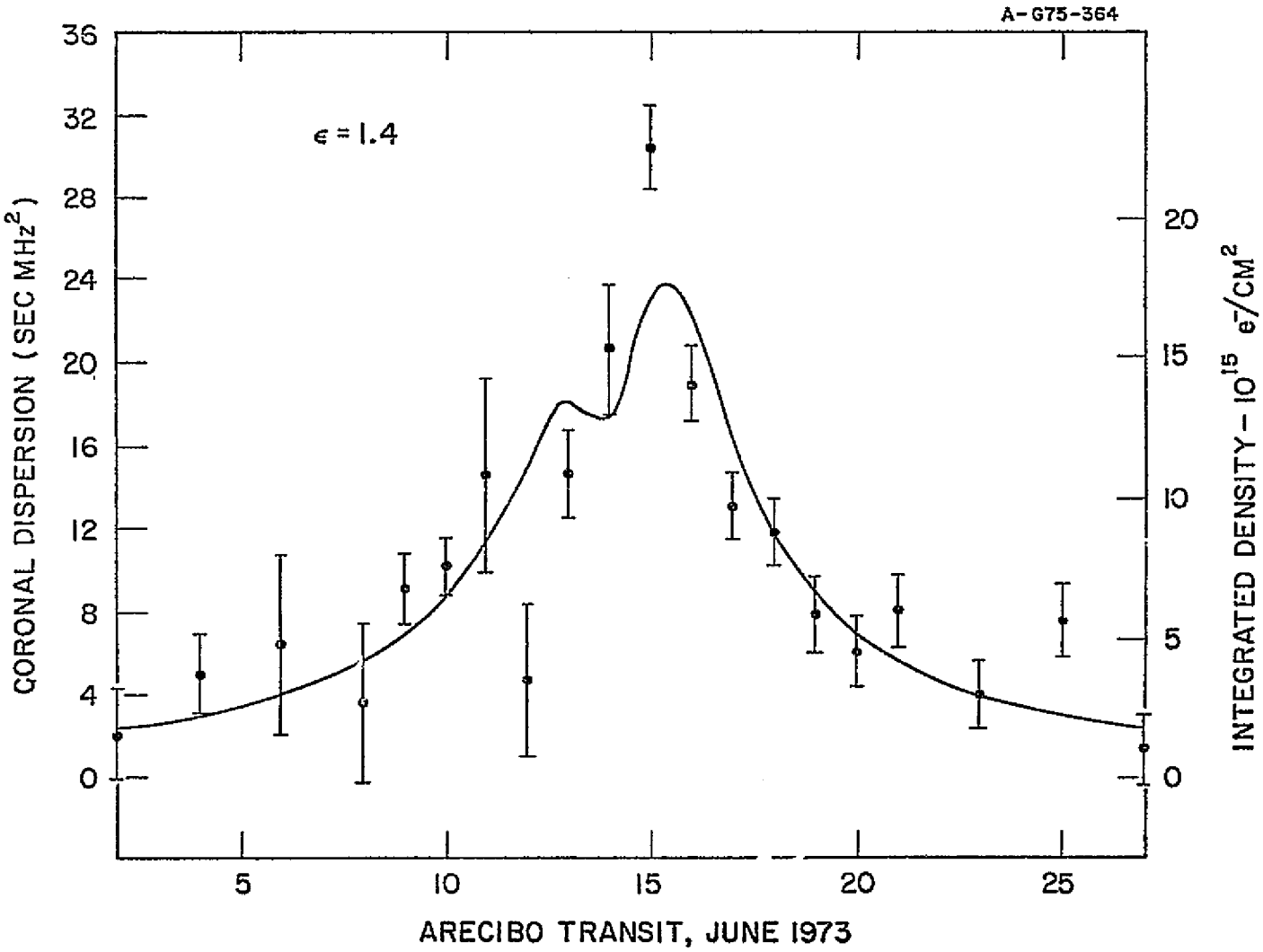
A-G75-364
ε = 1.4
CORONAL DISPERSION (SEC MHz²)
INTEGRATED DENSITY - 10¹⁵ e⁻/CM²
ARECIBO TRANSIT, JUNE 1973
0
4
8
12
16
20
24
28
32
36
5
10
15
20
25

Figure 12

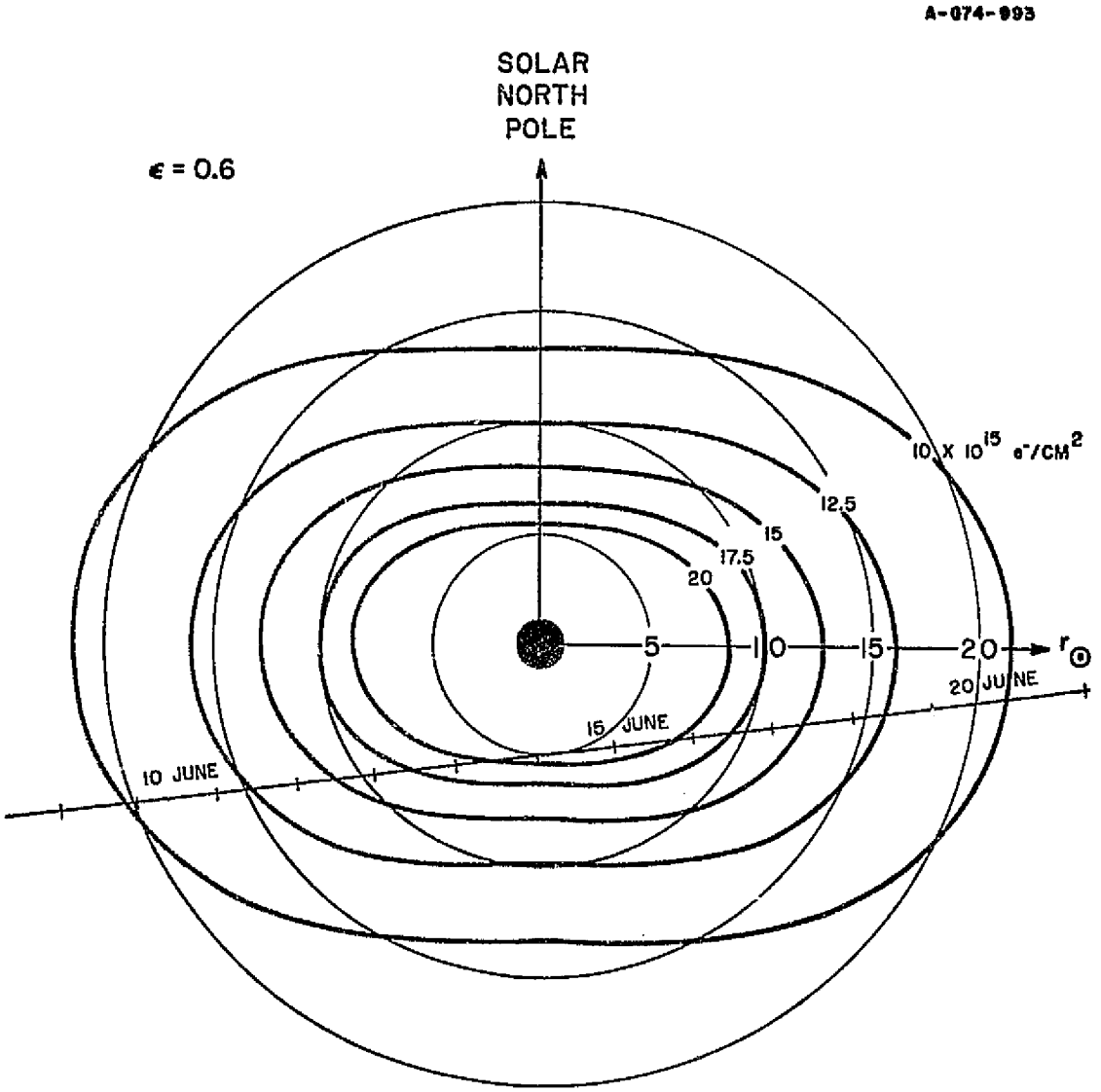
A-074-893
SOLAR
NORTH
POLE
ε = 0.6
10 X 10^15 e⁻/CM²
12.5
15
17.5
20
5
10
15
20
r⊙
20 JUNE
15 JUNE
10 JUNE

Figure 13

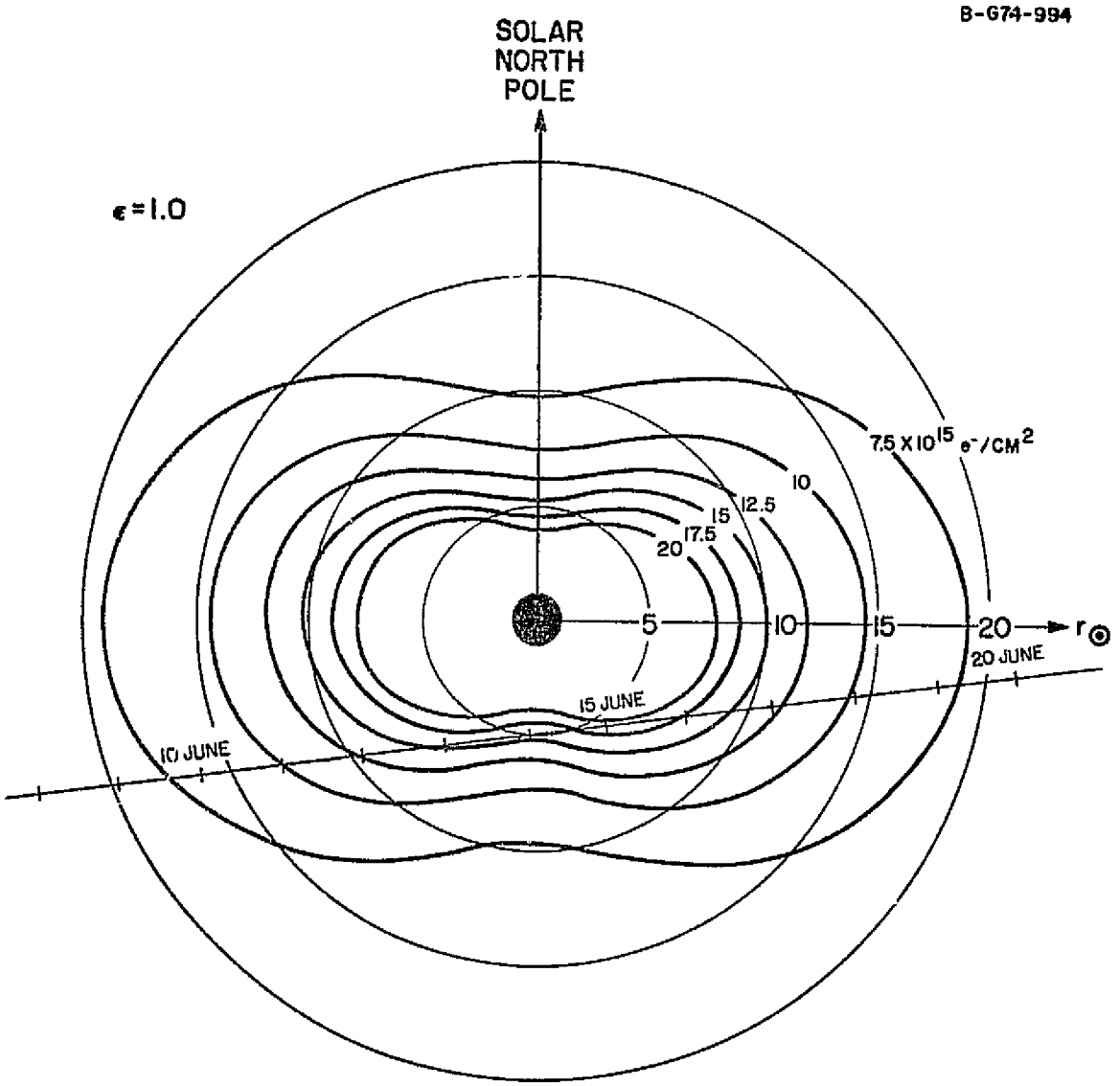

Figure 14

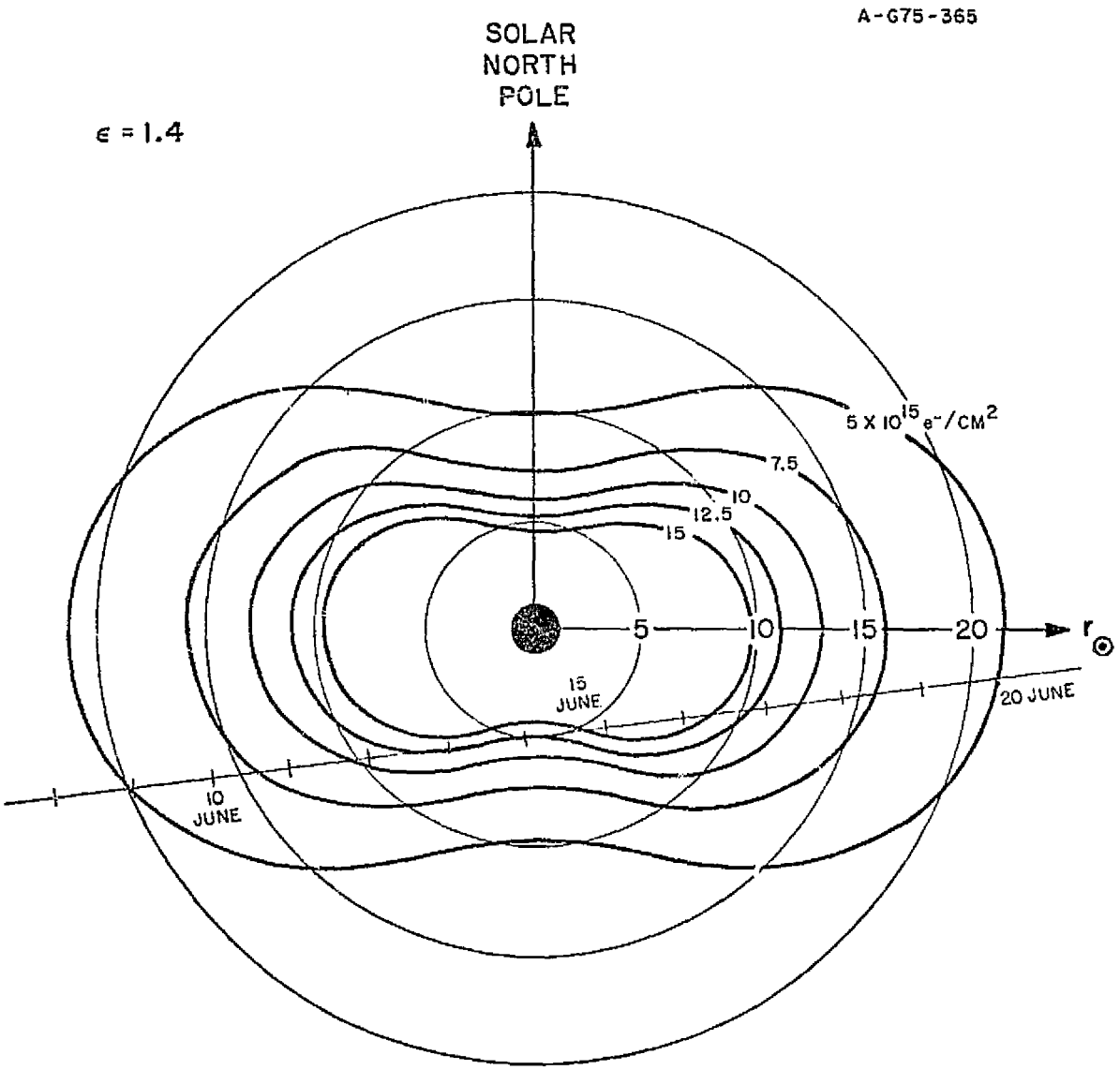
A-G75-365
SOLAR
NORTH
POLE
ε = 1.4
5 X 10^15 e⁻/CM²
7.5
10
12.5
15
5
10
15
20
r⊙
15
JUNE
20 JUNE
10
JUNE

Figure 15

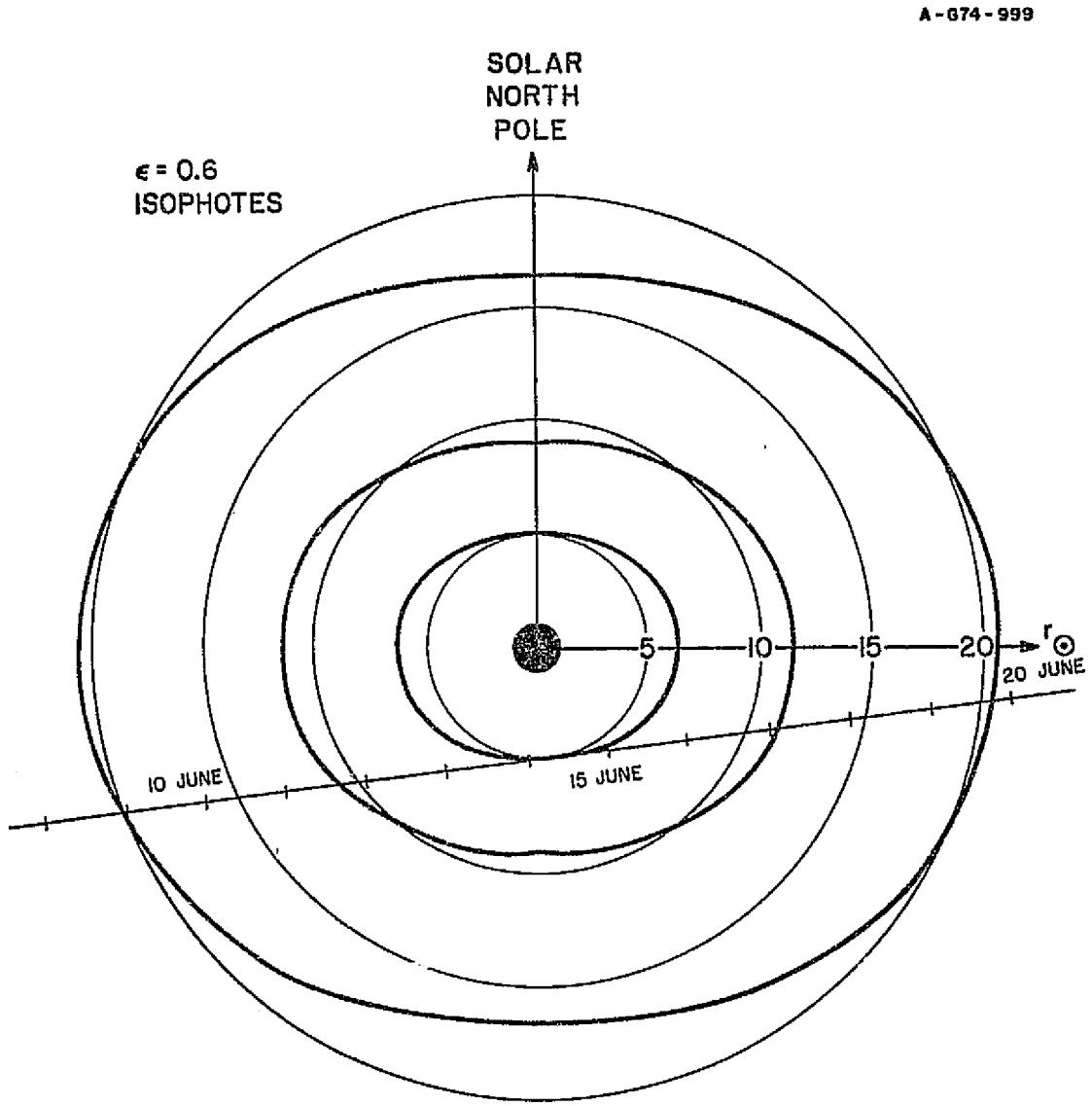

Figure 16

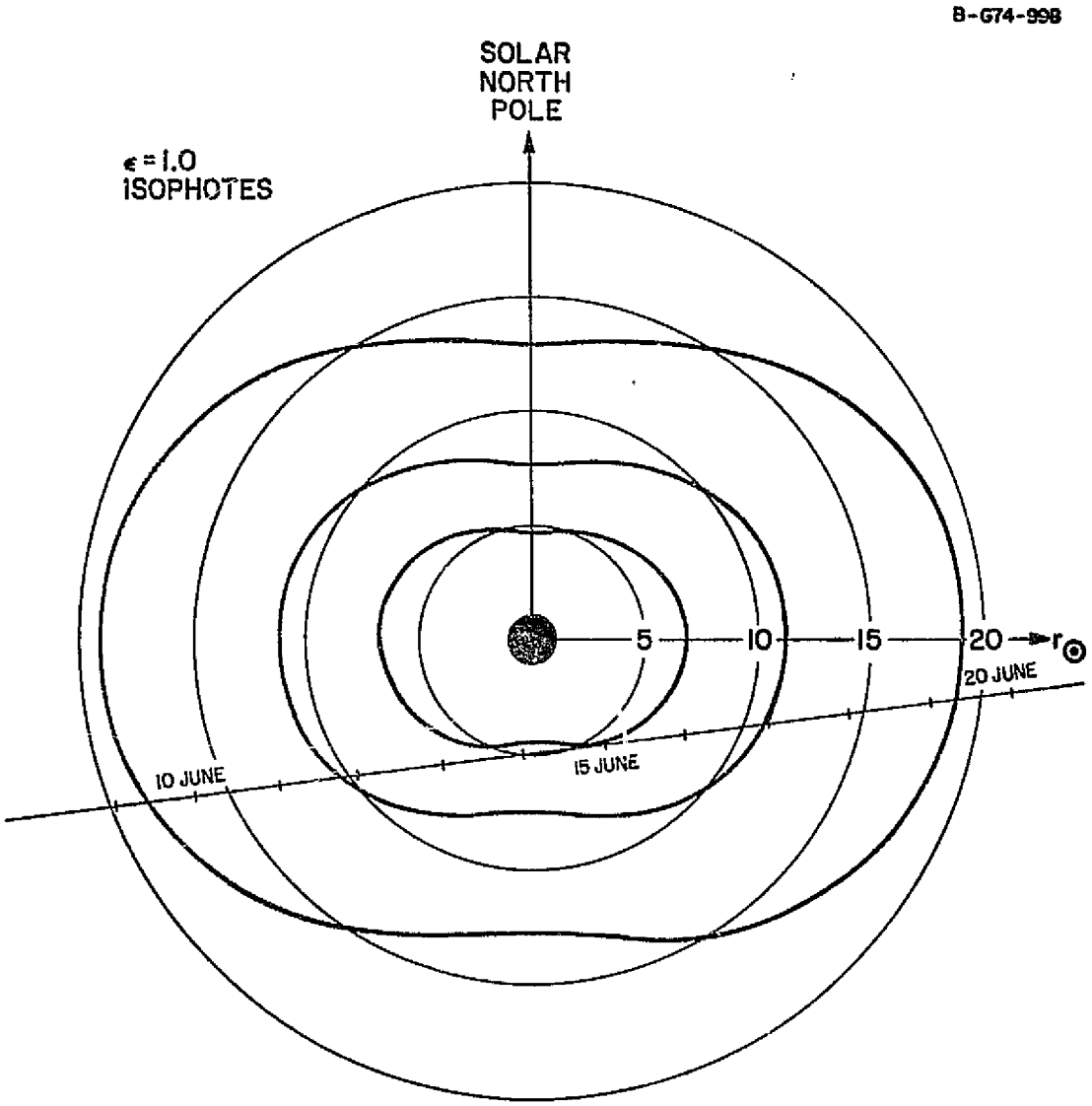
B-G74-998
SOLAR
NORTH
POLE
ϵ = 1.0
ISOPHOTES
5
10
15
20
r⊙
20 JUNE
15 JUNE
10 JUNE

Figure 17

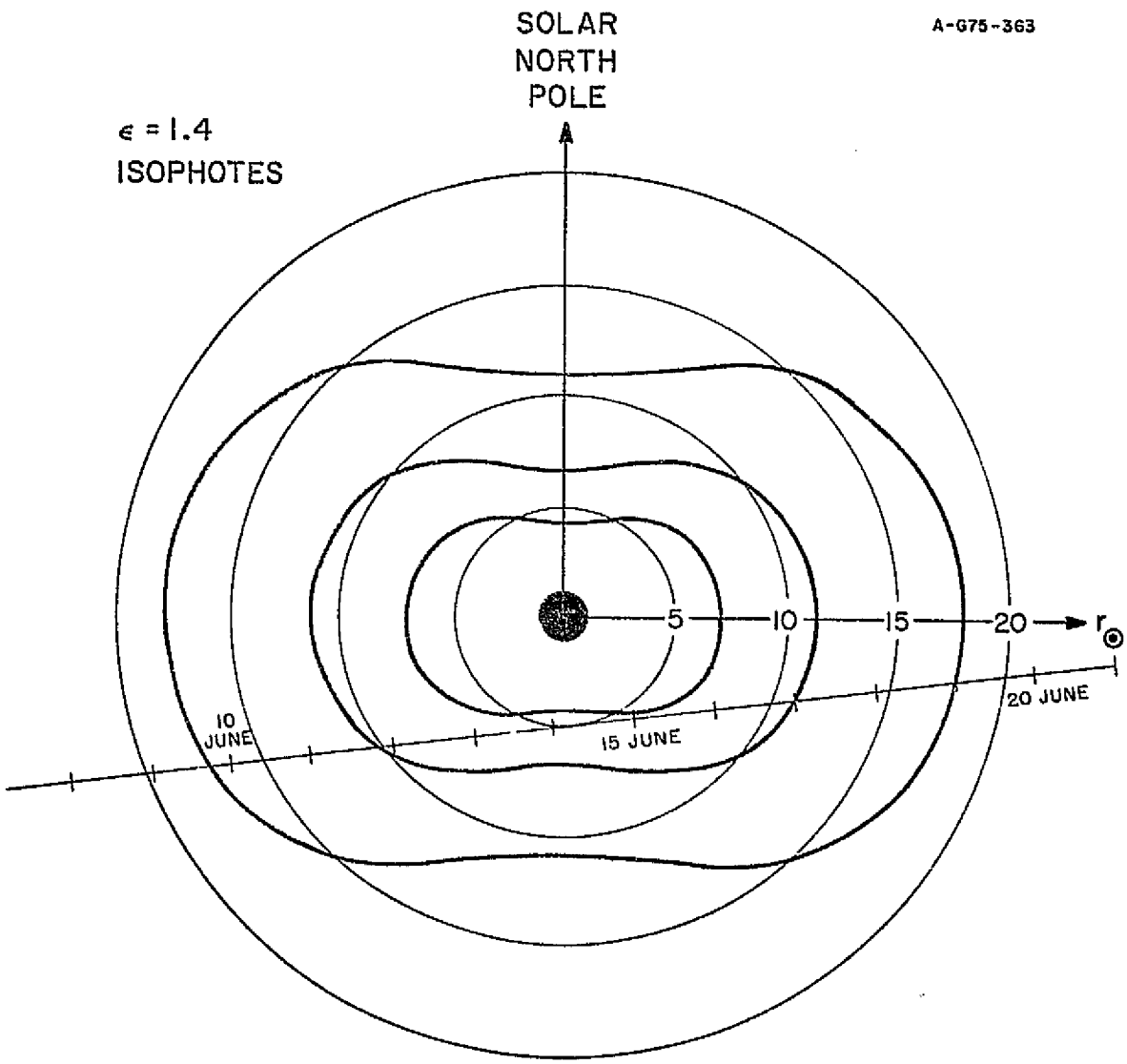
SOLAR
NORTH
POLE
A-G75-363
ε = 1.4
ISOPHOTES
5
10
15
20
r⊙
10
JUNE
15 JUNE
20 JUNE

Figure 18

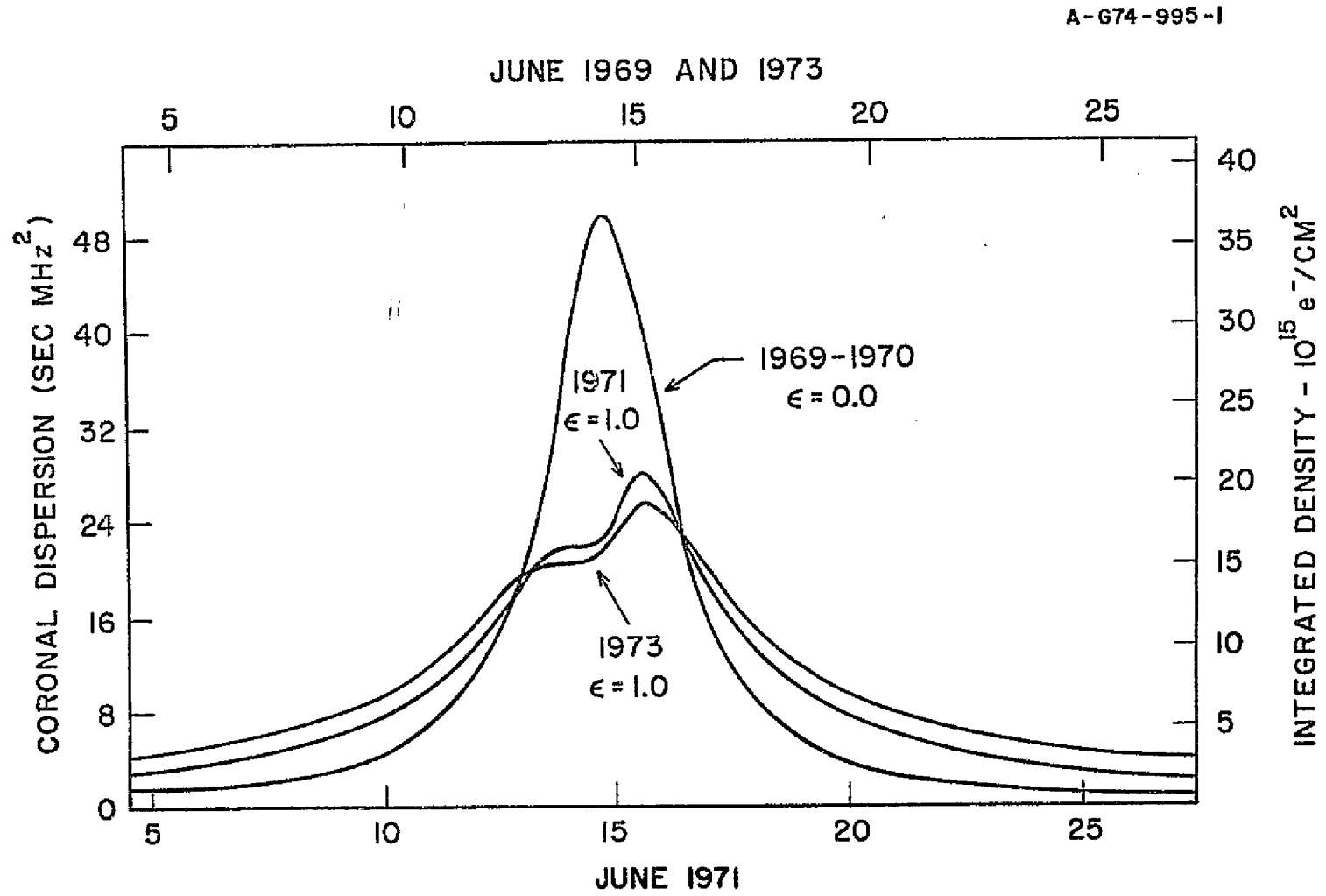

Figure 19